Article

Identification of NO$_2$ and SO$_2$ Pollution Hotspots and Sources in Jiangsu Province of China

Yu Wang [1,†] , **Md. Arfan Ali** [1,†] , **Muhammad Bilal** [1] , **Zhongfeng Qiu** [1,*] , **Alaa Mhawish** [1] , **Mansour Almazroui** [2,3] , **Shamsuddin Shahid** [4] , **M. Nazrul Islam** [2] , **Yuanzhi Zhang** [1] and **Md. Nazmul Haque** [5]

1   Lab of Environmental Remote Sensing (LERS), School of Marine Sciences (SMS), Nanjing University of Information Science and Technology (NUIST), Nanjing 210044, China; yuwang@nuist.edu.cn (Y.W.); md.arfanali@nuist.edu.cn (M.A.A.); muhammad.bilal@connect.polyu.hk (M.B.); alaa.mhawish@bhu.ac.in (A.M.); yzhang209@nuist.edu.cn (Y.Z.)
2   Center of Excellence for Climate Change Research, Department of Meteorology, King Abdulaziz University, Jeddah 21589, Saudi Arabia; mansour@kau.edu.sa (M.A.); mnislam@kau.edu.sa (M.N.I.)
3   Climatic Research Unit, School of Environmental Sciences, University of East Anglia, Norwich NR4 7TJ, UK
4   Department of Water and Environmental Engineering, School of Civil Engineering, Faculty of Engineering, Universiti Teknologi Malaysia (UTM), Johor Bahru 81310, Malaysia; sshahid@utm.my
5   Department of Urban and Regional Planning (URP), Faculty of Civil Engineering, Khulna University of Engineering and Technology, Khulna 9203, Bangladesh; nhaque13@urp.kuet.ac.bd
*   Correspondence: zhongfeng.qiu@nuist.edu.cn
†   These authors with equal contributions.

Abstract: Nitrogen dioxide (NO$_2$) and sulfur dioxide (SO$_2$) are important atmospheric trace gases for determining air quality, human health, climate change, and ecological conditions both regionally and globally. In this study, the Ozone Monitoring Instrument (OMI), total column nitrogen dioxide (NO$_2$), and sulfur dioxide (SO$_2$) were used from 2005 to 2020 to identify pollution hotspots and potential source areas responsible for air pollution in Jiangsu Province. The study investigated the spatiotemporal distribution and variability of NO$_2$ and SO$_2$, the SO$_2$/NO$_2$ ratio, and their trends, and potential source contribution function (PSCF) analysis was performed to identify potential source areas. The spatial distributions showed higher values (>0.60 DU) of annual mean NO$_2$ and SO$_2$ for most cities of Jiangsu Province except for Yancheng City (<0.50 DU). The seasonal analyses showed the highest NO$_2$ and SO$_2$ in winter, followed by spring, autumn, and summer. Coal-fire-based room heating and stable meteorological conditions during the cold season may cause higher NO$_2$ and SO$_2$ in winter. Notably, the occurrence frequency of NO$_2$ and SO$_2$ of >1.2 was highest in winter, which varied between 9.14~32.46% for NO$_2$ and 7.84~21.67% for SO$_2$, indicating a high level of pollution across Jiangsu Province. The high SO$_2$/NO$_2$ ratio (>0.60) indicated that industry is the dominant source, with significant annual and seasonal variations. Trends in NO$_2$ and SO$_2$ were calculated for 2005–2020, 2006–2010 (when China introduced strict air pollution control policies during the 11th Five Year Plan (FYP)), 2011–2015 (during the 12th FYP), and 2013–2017 (the Action Plan of Air Pollution Prevention and Control (APPC-AC)). Annually, decreasing trends in NO$_2$ were more prominent during the 12th FYP period (2011–2015: −0.024~−0.052 DU/year) than in the APPC-AC period (2013–2017: −0.007~−0.043 DU/year) and 2005–2020 (−0.002 to −0.012 DU/year). However, no prevention and control policies for NO$_2$ were included during the 11th FYP period (2006–2010), resulting in an increasing trend in NO$_2$ (0.015 to 0.031) observed throughout the study area. Furthermore, the implementation of China's strict air pollution control policies caused a larger decrease in SO$_2$ (per year) during the 12th FYP period (−0.002~−0.075 DU/year) than in the 11th FYP period (−0.014~−0.071 DU/year), the APPC-AC period (−0.007~−0.043 DU/year), and 2005–2020 (−0.015~−0.032 DU/year). PSCF analysis indicated that the air quality of Jiangsu Province is mainly influenced by local pollution sources.

Keywords: OMI; NO$_2$; SO$_2$; SO$_2$/NO$_2$ ratio; Jiangsu Province; trend

1. Introduction

China's rapid socio-economic development, industrialization, and urbanization have caused several severe environmental problems, including terrible air pollution [1–3]. Air pollutants are broadly categorized into two types, aerosol pollutants (as measured by aerosol optical depth (AOD) and particulate matter (PM)) and gaseous pollutants. PM is of significant concern to society and government due to its adverse health effects (e.g., cardiovascular and respiratory diseases) and environmental problems (e.g., smog that reduces atmospheric visibility) [4,5]. Gaseous pollutants (e.g., sulfur dioxide: SO_2; nitrogen dioxide: NO_2; and ozone: O_3) attract attention due to their significant effects on human health (e.g., asthma and cancer) and the atmospheric environment (e.g., deteriorating vegetation and forests, and global warming) [6–8].

The most important trace gases are NO_2 and SO_2, which play a significant role in the troposphere, resulting in several urban environmental pollution problems, such as acid rain, haze, and photochemical smog [9–12]. Kajino et al. [13] reported that secondary nitrate and sulfate particulates, formed by oxidation, affect the climate and radiative budget. In addition, they are responsible for the formation of acid rain, decreased crop production, and ecological damage [14,15]. NO_2 is produced from anthropogenic emissions (e.g., industrial burning of fossil fuels: coal, oil and gas, vehicle exhaust, biomass burning, and electricity production) and natural sources (soils through the decomposition process of nitrates and lightning) [16–19]. SO_2 is also produced from anthropogenic sources (e.g., burning of coal and oil fuels and the refinement of sulfide ores) as well as natural ones (intentional biomass burning and volcanic eruptions) [20,21]. The effect of NO_2 and SO_2 on human health and plants is well recognized. Motivated by these considerations, several researchers have investigated these two gaseous pollutants using ground and satellite observations [20–26].

Ground-based measurements can provide a correct and reliable picture of gaseous pollutants, offering insights into their temporal distributions and their effect on the climate and human health [20,23]. However, the ground-based stations have limited spatial distribution and sparse observations. Satellite-based remote sensing allows observation of long-term gaseous pollutants (e.g., NO_2 and SO_2) on national, regional, and global scales, overcoming the limitations of ground-based measurements in providing near-real-time (NRT) measurements with low-to-high spatial resolutions. The satellite-based observations also allow the study of long-distance transportation of NO_2 and SO_2 [27] and the contributions from different sources [28,29]. Several satellite sensors, such as the Global Ozone Monitoring Instrument (GOME) [30,31], the Scanning Imaging Absorption spectrometer for Atmospheric CHartographY (SCIAMACHY) [32], GOME-2 [33,34], the Ozone Monitoring Instrument (OMI) [35,36], and the TROPOspheric Monitoring Instrument (TROPOMI) [37], have been designed to get accurate information about atmospheric pollutants. Krotkov et al. [21] and Levelt et al. [38] reported that OMI is the most commonly used sensor, with high spatial (13 km × 24 km, at nadir) and temporal (98.8 min) resolutions. Levelt et al. [38] also reported extensive use of OMI sensors for monitoring air quality (e.g., NO_2, SO_2, aerosols, and HCHO), detection of ozone (O_3), volcanoes, and solar radiation. Damiani et al. [39] evaluated OMI-, GOME-, and SCIAMACHY-based ozone against ground-based ozone over the Arctic regions and found good agreement between satellite and ground measurements. Krotkov et al. [21] studied changes in OMI-based NO_2 and SO_2 pollution over the United States, Asia, and Europe from 2005 to 2015 and found both increasing and decreasing trends in NO_2 and SO_2, depending on the region. Celarier [40] evaluated OMI-based NO_2 with ground-based measurements and found correlations between 0.8 and 0.9 on a global scale. Penn and Holloway [41] evaluated GOME- and OMI-based NO_2 over the United States and reported consistent correlations with surface measurements (GOME: 0.61 and OMI: 0.59). Lamsal et al. [42] evaluated NO_2 trends based on the ground measurement and the OMI-based tropospheric NO_2 vertical column density (VCD) over the United States. Haq et al. [22] studied spatiotemporal distributions and variations of OMI-based NO_2 and its trends over South Asia from 2004 to 2015.

Several earlier studies have also investigated and validated the spatiotemporal distribution and variability of OMI-based NO_2 and SO_2 and their trends over China [20,23,43–50]. For example, Wang et al. [49] validated both OMI- and TROPOMI-based NO_2 against MAX-DOAS over China and found correlations above 0.8 and 0.95 for daily and monthly scales, respectively. In addition, Zheng et al. [23] evaluated OMI-based NO_2 and SO_2 against surface measurements over Inner Mongolia and found correlations of 0.897 and 0.696 for NO_2 and SO_2, respectively. Wang et al. [50] validated OMI, GOME-2A, and GOME-2B tropospheric NO_2 and SO_2 against MAX-DOAS products from 2011 to 2014, and found an R^2 of 0.73, 0.33, and 0.20 for OMI, GOME-2A, and GOME-2B, respectively, over Wuxi, China. Apart from these, Li et al. [47] investigated OMI-based SO_2 over China from 2005 to 2007 and reported significant reductions of SO_2 from Chinese power plants. Li et al. [48] re-investigated the OMI-based SO_2 in 2017 and found a 75% reduction since 2007. Liu et al. [44] studied both OMI and emission inventory-based NO_2 over China and reported a decrease in column NO_2 of 32% from 2011 to 2015. In 2017, Liu et al. [45] again studied the trend in NO_2 emitted from power plants across China and reported a 52% increase during 2005–2011 and a 21% decrease during 2011–2015. Van der A et al. [43] calculated NO_2 and SO_2 trends and used these to evaluate the effectiveness of the air quality policy in China. Zhang et al. [20] investigated the spatiotemporal distribution and variability of OMI-based NO_2 and SO_2 and calculated their trends from 2005 to 2014 over Henan Province of China. Cui et al. [46] found a rapid increase in NO_2 over western China and Inner Mongolia from 2005 to 2013. Song et al. [51] studied the temporal distribution of air pollution (e.g., CO, NO_2, SO_2, PM2.5, and PM10) using surface data and investigated their relationships with meteorological parameters in Jiangsu Province, China, from 2013 to 2017. They did not present any spatial distribution, variations, or trends in CO, NO_2, SO_2, PM2.5, and PM10, which is a limitation of their study. Spatial distributions help to better understand air pollution scenarios; what is occurring in air pollution and where it is happening. With this in mind, the present study considered Aura-OMI-retrieved NO_2 and SO_2 products to identify their hotspots (e.g., spatial distributions, variations, and temporal changes) and to locate their sources using the potential source contribution functions (PSCF) analysis over Jiangsu Province.

In 2016, Yale University published the Environmental Performance Index (EPI) report, which ranked China as of last in the world, just before Bangladesh, based on air quality assessment [52,53]. Jiangsu Province is an economically developed province in eastern China, having dense metropolises and large rural areas, with urban constructions, high traffic volumes, industrial production, and crop residue burning, which all add significant amounts of pollutants into the atmosphere, resulting in noticeable air pollution in the province [1]. This province is located between the northern and southern parts of China, in a region known as the climate transition zone. It is also located between the Yangtse River Delta and the BTH, where air pollution occurs frequently. According to Jiangsu's Environmental Status Bulletin (2012–2015), the 13 cities of Jiangsu Province did not reach the national air quality standard. Therefore, a study related to identifying NO_2 and SO_2 pollution hotspots and sources in Jiangsu Province of China is necessary. To the best of our knowledge, not a single study has identified pollution hotspots using long-term (2005–2020) NO_2 and SO_2 data as well as their main sources at a local scale in Jiangsu Province of China. The present study has two main objectives: (1) to study long-term spatiotemporal distributions and variations of NO_2 and SO_2, including their ratio, and trends and (2) to identify their potential source areas using the potential source contribution function (PSCF). This study provides insight into the interaction's atmospheric gaseous pollutants in order to understand air quality issues at the city level.

2. Materials and Methods

2.1. Study Area

China is the largest country among all the Asian countries and has the largest population globally. The country has different administrative boundaries, such as 2 administrative regions

(Hong Kong and Macau), 4 municipalities (Chongqing, Beijing, Shanghai, and Tianjin), 5 autonomous regions, and 23 provinces. Jiangsu Province, a fully developed region, is known for its unique cultural, economic, and political activities. The province is located between 116°18′–121°57′ E and 30°45′–35°20′ N and has an area of 102,600 km^2. Jiangsu Province is located in eastern China and covers most of the Yangtse River Delta (YRD). Jiangsu Province is agriculturally highly productive, which results in its high population density (with a total population of around 80 million). Since the economic reforms of 1990, Jiangsu Province has become a hotspot for its economic development, ranking the province at the top in per capita GDP. The province is home to some of the world's leading exporters of chemicals, electronic equipment, and textiles companies, located in its 13 major cities (Figure 1).
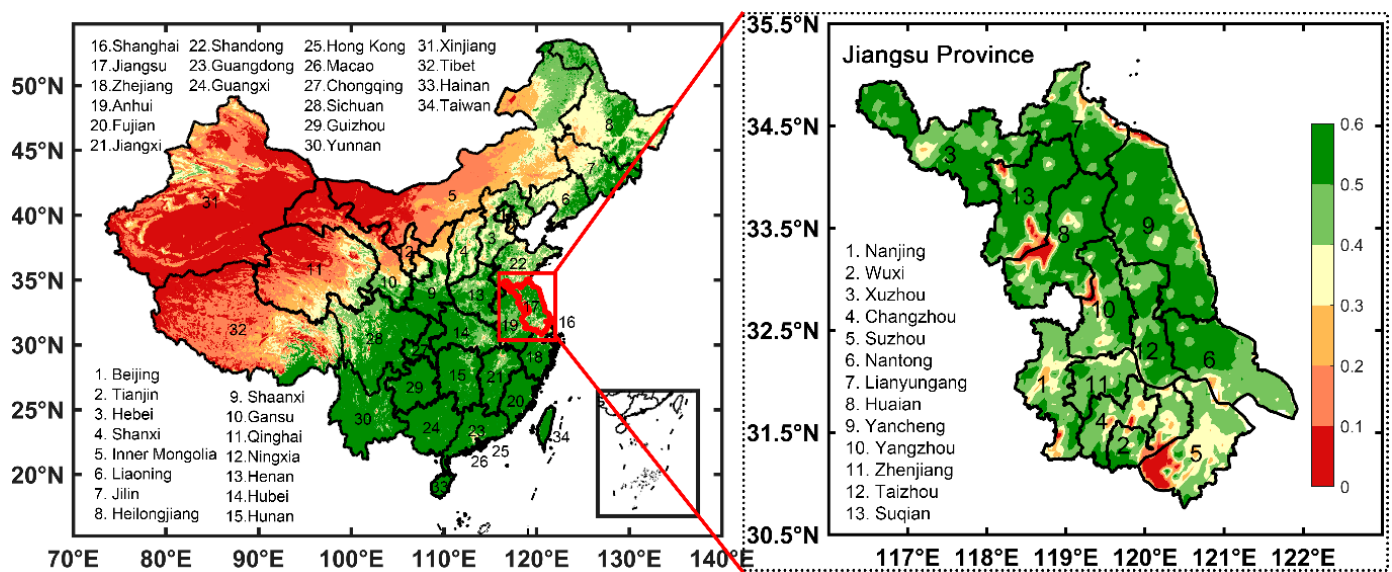

Figure 1. Map of NDVI for Jiangsu Province, China, with major cities. The background image reveals the multi-year (2005−2020) averages of MODIS NDVI, with arid surfaces (NDVI < 0.2), lighter or sparse vegetation (0.2 < NDVI < 0.4), moderate vegetation (0.4 < NDVI < 0.5), and dark vegetation (NDVI > 0.5).

Most areas of Jiangsu Province have a humid continental climate. The annual mean temperature varies from 13 °C to 16 °C. The 16-year (2005–2020) precipitation data were downloaded from the Global Precipitation Measurement (GPM: GPM_3IMERGM_06; https://giovanni.gsfc.nasa.gov/; accessed on 15 March 2021), and we found that the annual mean precipitation varies from 936.52 mm/year to 1576.51 mm/year. The amounts of seasonal precipitation (mm/season) are about 144.16 for winter, 215.47 for spring, 607.46 for summer, and 233.79 for autumn. The province has four distinct seasons: December to February for winter, March to May for spring, June to August for summer, and September to November for autumn. The winter monthly average temperature varies from −1 °C to 4 °C, and the summer monthly average temperature is between 26 °C and 29 °C. Heavy rainfalls are recorded in spring and summer, and typhoons bring rainstorms during late summer and autumn.

2.2. OMI Data

The Ozone Monitoring Instrument (OMI), flies on the Aura sun-synchronous satellite, tracking at 705 km altitude, and was launched on 15 July 2004. Its crossing time is about 01:45 p.m. (local time). It is a hyperspectral sensor that measures the reflected radiation from the earth–atmosphere system using wavelengths of 250–500 (nm), with daily global coverage at a spatial resolution of 13 × 25 km at nadir. The OMI sensor uses an algorithm of OMAERUV to retrieve absorbing aerosol optical depth (AAOD, 388 nm), the ultraviolet aerosol index (UVAI), the AOD, and the SSA [54–56]. This sensor also provides atmospheric

trace gases (e.g., O_3, NO_2, and SO_2) [21,57–62]. In this study, long-term (2005−2020) OMAERUV version 3, level 3 daily cloud-screened (cloud fraction < 30%) total column NO_2 (OMNO2d) and SO_2 (cloud radiance fraction < 0.2, OMSO2e) products at a spatial resolution of $0.25° \times 0.25°$ were used.

2.3. Research Methodology

The following methodology was adopted to identify NO_2 and SO_2 (DU) pollution hotspots and their potential source areas in Jiangsu Province:

- The daily OMI-based NO_2 and SO_2 data were averaged to seasonal and annual scales. For annual and seasonal analysis, point data for 13 cities and the entire Jiangsu Province were extracted using the city-level shapefile.
- The Mann–Kendal test was used to calculate trends, while Sen's slope method was used to derive the magnitudes of NO_2 and SO_2 trends. The following steps were used to calculate trends:

If $x_1, x_2, x_3 \ldots \ldots x_i$ represent n data points where x_i represents the data point at time i, then the Mann–Kendall statistic and Sen's slope (S, Equations (1) and (2)) is given by [63,64]

$$S = \sum_{k=1}^{n-1} \sum_{i=k+1}^{n} \text{sign}(x_i - x_k) \tag{1}$$

where

$$\text{sign}(x_i - x_k) = \begin{cases} 1, & \text{if } (x_i - x_k) > 0 \\ 0, & \text{if } (x_i - x_k) = 0 \\ -1, & \text{if } (x_i - x_k) < 0 \end{cases} \tag{2}$$

The probability associated with S and the sample size, n, were calculated to quantify the significance of NO_2 and SO_2 trends based on the normalized statistics (Z, Equation (3)):

$$Z = \begin{cases} \frac{S-1}{\sqrt{\text{VAR(S)}}}, & \text{if } S > 0 \\ 0, & \text{if } S = 0 \\ \frac{S-1}{\sqrt{\text{VAR(S)}}}, & \text{if } S < 0 \end{cases} \tag{3}$$

At the 95% significance level, the null hypothesis of no trend is rejected if $|Z| > 1.96$.

Sen's slope [65] method was applied to derive the slope as a measure of change per unit time (Equation (4)):

$$Q' = \frac{x_{t'} - x_t}{t' - t} \tag{4}$$

where Q'= slope between data points $x_{t'}$ and x_t, $x_{t'}$ = data measurement at a time t', and x_t = data measurement at time t.

Sen's estimator of the slope is acquired based on the median slope

$$\begin{aligned} Q &= Q'[N+1/2] & \text{if N is odd} \\ &= \left(Q'_{[N/2]} + Q'_{[(N+2)/2]} \right)/2 & \text{if N is even} \end{aligned} \tag{5}$$

where N is the number of calculated slopes.

- The Hybrid Single-Particle Lagrangian Integrated Trajectory (HYSPLIT) model from the US National Oceanic and Atmospheric Administration (NOAA) [66] is a complete dispersion, transport, and chemical transformation model. This HYSPLIT model has been used to discover the sources of air masses using back-trajectory analysis [67], and PSCF analysis represents the potential sources of gaseous pollutants impacting China's air quality. In this study, 72 h HYSPLIT back trajectories at 500 m above ground level (AGL) were calculated for every hour at seasonal scales from 2014 to 2020 using the Global Data Assimilation System (GDAS)-based meteorological data with a spatial resolution of $1° \times 1°$ (link: ftp://arlftp.arlhq.noaa.gov/pub/archives/

gdas1, accessed date: 25 July 2021). Begum et al. [68] reported that 500 m height is suitable for representing pollution as it is the representative height of the mixed layer. MeteoInfo TrajStat software [69] in conjunction with HYSPLIT and MATLAB were used to compute the back-trajectory clustering and investigate the origins of gaseous pollutants (NO_2 and SO_2) in Jiangsu Province. The typical lifetime of NO_2 (SO_2) is around 6 h (15 h) in summer and 21 h (65 h) in winter [70,71]; therefore, in this study, PSCF analysis was based on 72 h back trajectory from the HYSPLIT model combining with hourly surface measurements. The PSCF analysis used hourly surface-based NO_2 and SO_2 concentrations over a grid size of 0.5 × 0.5 degrees. Furthermore, the study used 1 hourly MEP-based surface NO_2 and SO_2 data from 91 sites in 13 cities of Jiangsu Province (link: http://106.37.208.233:20035/, accessed date: 25 July 2021). The PSCF value was calculated based on the assumption that the trajectory endpoint is located within a grid cell (i, j), and the trajectory was assumed to collect pollutants emitted from different pocket emission sources within that cell (i, j). The PSCF value can be explained as a conditional probability that defines the potential contributions of a grid cell to the high NO_2 and SO_2 loadings at the receptor sites. The value of the PSCF for the ijth grid cell is calculated based on the following Equation (6):

$$PSCF = \frac{m_{ij}}{n_{ij}} \tag{6}$$

where n_{ij} is the number of endpoints that fall or pass through the ijth cell and m_{ij} defines the number of endpoints in the ijth cell having a concentration higher than an arbitrarily set criterion of the 75 percentile. For the two pollutants NO_2 and SO_2, the thresholds were 46.875 $\mu g/m^3$ and 20.143 $\mu g/m^3$, respectively. To reduce the uncertainty of the PSCF that resulted from small n_{ij}, an arbitrary weight function ($W_{i,j}$) is multiplied into the PSCF (Equation (7)):

$$W_{i,j} = \begin{cases} \text{if } n_{ij} > 3\overline{n} \rightarrow 1.00 \\ \text{if } 1.5\overline{n} < n_{ij} \leq 3\overline{n} \rightarrow 0.70 \\ \text{if } \overline{n} < n_{ij} \leq 1.5\overline{n} \rightarrow 0.42 \\ \text{if } n_{ij} \leq \overline{n} \rightarrow 0.15 \end{cases} \tag{7}$$

Here, n = average number of endpoints, which is calculated for each cell that has at least one endpoint. Hence, the weighted PSCF (WPSCF) is computed using Equation (8):

$$WPSCF = W_{i,j} \times PSCF \, (i, j) \tag{8}$$

Several studies [1,62,68,69] have also used the above-mentioned methods in air quality data analysis.

3. Results and Discussion

3.1. Spatial Distributions of NO_2 and SO_2

Fossil fuel combustion, industrial emissions, automobile emissions, biomass burning, natural lightning, and soil microbe emissions are the main sources of NO_2 [16,17,62,72]. In contrast, volcanoes, coal, oil and gas, and smelters are the major contributors to anthropogenic SO_2 emissions [72]. Figure 2 shows the annual and seasonal spatial distribution of OMI-based NO_2 and SO_2 in Jiangsu Province from 2005 to 2020. The spatial distributions of annual mean NO_2 and SO_2 were high (>0.60 DU) in most cities of Jiangsu Province except for Yancheng City (<0.50 DU). For the 13 studied cities, the 16-year city-level annual mean NO_2 concentration was highest in Wuxi (0.78 ± 0.09 DU) and lowest in Yancheng (0.46 ± 0.05 DU) (Table 1). In contrast, the annual mean SO_2 was highest in Xuzhou (0.63 ± 0.16) and lowermost in Yancheng (0.48 ± 0.08 DU) (Table 1). Notably, the NO_2 and SO_2 values for 13 cities were close to each other, indicating the existence of significant gaseous pollutant emissions in Jiangsu Province (NO_2 = 0.58 ± 0.06 DU and SO_2 = 0.56 ± 0.11 DU), which are strongly impacted by the intense anthropogenic emis-

sions, resulting in high NO_2 and SO_2. High NO_2 pollution is attributed to the dense population and unsustainable anthropogenic emissions from mobile sources [73]. Song et al. [51] reported that the cities of southern Jiangsu (e.g., Changzhou, Nanjing, Suzhou, Wuxi, and Zhenjiang) are host to many industries and have high traffic volumes, resulting in high NO_2 and SO_2 over these cities. A significant increase in industrial development and traffic over eastern China is another important reason for increasing NO_2 [74,75]. Li et al. [76] reported that industry was the top source of NO_2 emission (39%) in China in 2010, followed by power plants (32%), traffic (25%), and residential activities (4%). Apart from these, Luo et al. [59] reported that long-term exposure to NO_2 is responsible for significant increases in China's respiratory and cardiovascular mortality rates. In addition, Dahiya and Myllyvirta [72] reported that China is the third-largest emitter in the world due to having the highest number of coal-fired power plants (total number of coal-fired plants = 86). The coal-fired industry (steel), power plants, and manufacturing companies are located mainly in Changzhou–Wuxi (SO_2 emission in 2018: 47 kilotons/year), Tangshan–Xuzhou (31 kilotons/year), and Nanjing (24 kilotons/year) [72].

Seasonally, spatial NO_2 and SO_2 (DU) were highest in winter followed by spring, autumn, and summer (Figure 2), in line with the findings of three earlier studies over different parts of China [77], including 10 background and rural sites in China [78], Henan Province [20], Inner Mongolia [23], and Shanghai and Chongming Eco-Island [79], China. In winter, the hotspots of NO_2 and SO_2 (DU) were observed in most parts of Jiangsu Province except for Yancheng City, as indicated by high values of NO_2 and SO_2 (>0.75 DU). Perhaps coal-fired room heating and stable meteorological conditions during the winter season are responsible for high NO_2 and SO_2 in the study area [20]. In addition, Zhang et al. [20] reported that the cold weather in winter could result in limited radical formation with less NOx washing out from the atmosphere. In spring, the spatial hotspots of NO_2 and SO_2 were observed in most cities of Jiangsu Province, as indicated by high values of NO_2 and SO_2 (0.60~0.90 DU). Similar patterns were also noticed during the autumn. Plenty of precipitation in summer might contribute significantly to the low concentration of NO_2 and SO_2 throughout Jiangsu Province, in line with the findings of Zheng et al. [23] in Inner Mongolia. Feng et al. [80] reported that the wet deposition of precipitation substantially decreases the pollutants in the atmosphere. Remarkably, all the 13 studied cities had higher NO_2 (DU) in winter (0.66~1.05), followed by autumn (0.42~0.81), spring (0.45~0.83), and summer (0.29~0.45), while SO_2 concentrations were also higher in winter (0.61~0.85) than in spring (0.54~0.69), autumn (0.45~0.65), and summer (0.28~0.46) (Table 1).

3.2. Frequency Distributions of NO_2 and SO_2

Figure 3 represents the annual and seasonal frequency distribution of OMI-based total column NO_2 and SO_2 (DU) based on daily datasets for 13 cities of Jiangsu Province from 2005 to 2020. During the study period, at an annual scale, the bin of 0.0–0.15 for NO_2 and SO_2, signifying low pollution levels, showed an occurrence frequency for NO_2 of <1.67% and for SO_2 of <10.82% throughout the 13 cities of Jiangsu Province (Figure 3). NO_2 and SO_2 occurrence frequencies substantially increased to the 0.30−0.45 bin and then gradually decreasing from the 0.45–0.60 bin, reaching their lowest in the 1.05−1.20 bin. In particular, the occurrence frequencies of the $0.30 \leq NO_2 < 0.45$ bin were comparatively highest in Huaian (31.25%) and lowest in Wuxi, whereas the occurrence frequencies of $0.30 \leq SO_2 < 0.45$ were relatively highest in Yancheng (21.99%) and lowest in Taizhou. Moreover, the occurrence frequencies of the $0.40 \leq NO_2 < 0.60$ bin were somewhat higher in Nanjing (19.26%) and reached their lowest in Yancheng. The same bin for SO_2 had its highest occurrence frequency in Yangzhou (16.88%) and lowest in Wuxi. The 0.3–0.45 and 0.45–0.60 bins were well occupied, indicating a moderate level of pollution for the 13 cities of Jiangsu Province. For the 1.05−1.20 bin, the occurrence frequency of NO_2 was highest in Suzhou (7.27%) and lowest in Yancheng, whereas SO_2 was somewhat highest in Wuxi (5.56%) and lowest in Yancheng, indicating a high level of pollution throughout the study area.
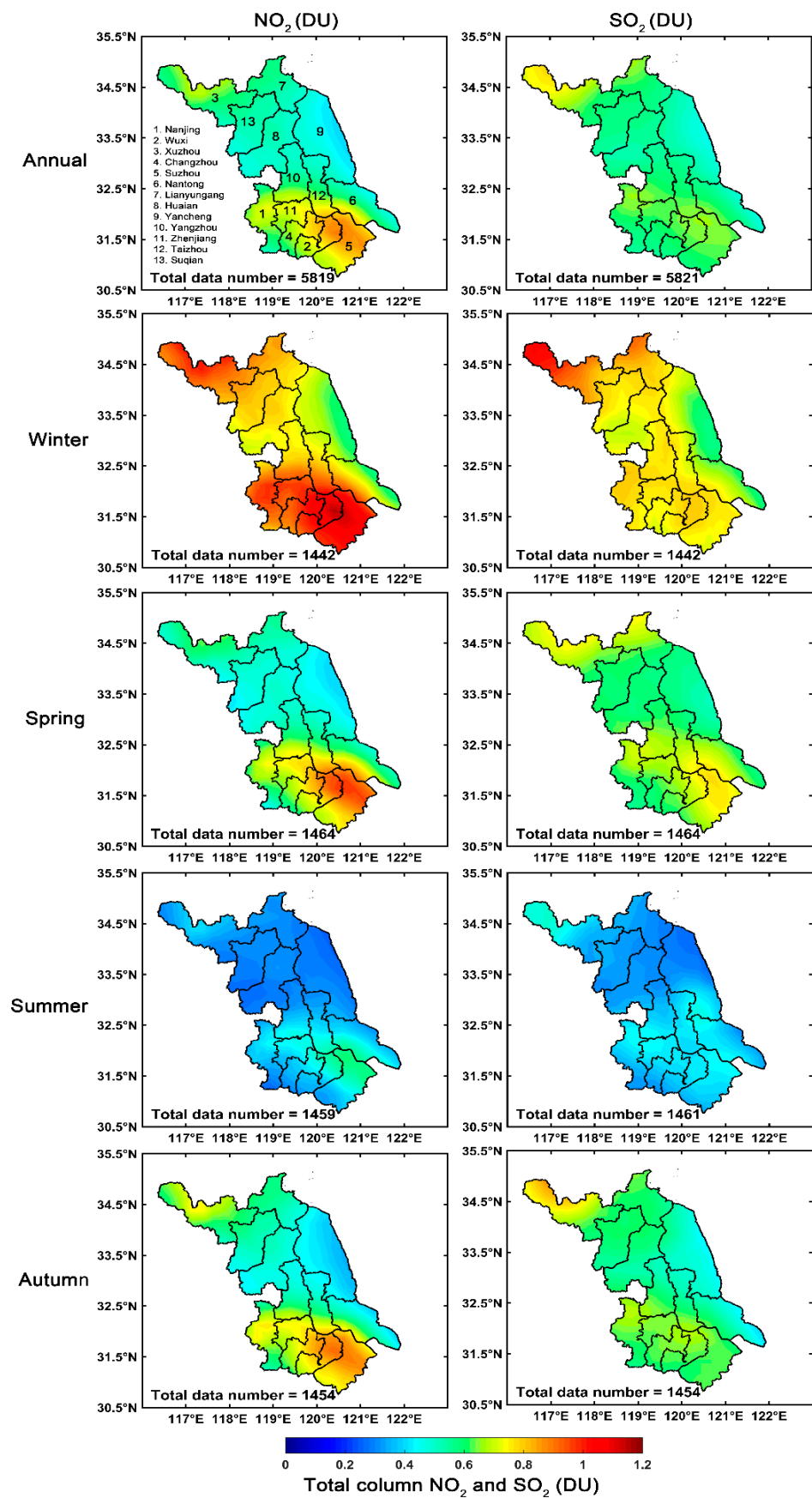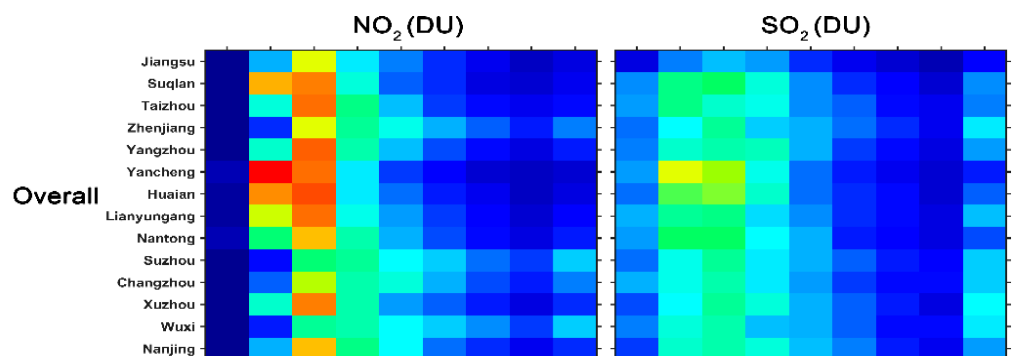
Figure 2. Annual and seasonal spatial distribution of OMI-retrieved NO$_2$ (DU) and SO$_2$ (DU) over Jiangsu Province from 2005 to 2020.

Table 1. The city-averaged seasonal and annual mean NO_2 and SO_2 ($\pm$STD) (DU) obtained from OMI from 2005 to 2020 in 13 cities of Jiangsu Province.

	Annual		Winter		Spring		Summer		Autumn	
	NO_2	SO_2	NO_2	SO_2	NO_2	SO_2	NO_2	SO_2	NO_2	SO_2
Nanjing	0.64 ± 0.08	0.58 ± 0.11	0.92 ± 0.14	0.75 ± 0.17	0.63 ± 0.10	0.60 ± 0.14	0.35 ± 0.04	0.37 ± 0.12	0.66 ± 0.07	0.60 ± 0.17
Wuxi	0.78 ± 0.09	0.61 ± 0.15	1.05 ± 0.13	0.72 ± 0.21	0.82 ± 0.10	0.68 ± 0.19	0.44 ± 0.05	0.42 ± 0.14	0.81 ± 0.09	0.60 ± 0.18
Xuzhou	0.61 ± 0.07	0.63 ± 0.16	0.92 ± 0.15	0.85 ± 0.25	0.54 ± 0.08	0.64 ± 0.19	0.33 ± 0.02	0.38 ± 0.12	0.64 ± 0.07	0.65 ± 0.24
Changzhou	0.71 ± 0.08	0.57 ± 0.13	0.99 ± 0.14	0.70 ± 0.18	0.73 ± 0.12	0.61 ± 0.16	0.39 ± 0.04	0.35 ± 0.08	0.75 ± 0.09	0.60 ± 0.18
Suzhou	0.78 ± 0.08	0.61 ± 0.15	1.04 ± 0.16	0.71 ± 0.20	0.83 ± 0.10	0.69 ± 0.19	0.45 ± 0.04	0.43 ± 0.15	0.80 ± 0.07	0.62 ± 0.17
Nantong	0.57 ± 0.06	0.51 ± 0.10	0.73 ± 0.12	0.61 ± 0.13	0.62 ± 0.08	0.61 ± 0.16	0.42 ± 0.04	0.37 ± 0.15	0.52 ± 0.07	0.46 ± 0.10
Lianyungang	0.54 ± 0.05	0.56 ± 0.13	0.82 ± 0.11	0.77 ± 0.18	0.51 ± 0.07	0.62 ± 0.17	0.31 ± 0.02	0.29 ± 0.09	0.53 ± 0.06	0.54 ± 0.17
Huaian	0.50 ± 0.05	0.51 ± 0.09	0.75 ± 0.11	0.69 ± 0.14	0.47 ± 0.07	0.55 ± 0.15	0.29 ± 0.01	0.28 ± 0.05	0.47 ± 0.04	0.52 ± 0.13
Yancheng	0.46 ± 0.05	0.48 ± 0.08	0.66 ± 0.11	0.63 ± 0.12	0.45 ± 0.07	0.54 ± 0.13	0.30 ± 0.01	0.28 ± 0.06	0.42 ± 0.05	0.45 ± 0.09
Yangzhou	0.58 ± 0.06	0.56 ± 0.12	0.82 ± 0.11	0.75 ± 0.21	0.60 ± 0.09	0.62 ± 0.18	0.36 ± 0.04	0.32 ± 0.07	0.54 ± 0.06	0.53 ± 0.15
Zhenjiang	0.71 ± 0.09	0.62 ± 0.13	0.97 ± 0.14	0.74 ± 0.18	0.73 ± 0.12	0.65 ± 0.17	0.42 ± 0.05	0.46 ± 0.12	0.73 ± 0.09	0.61 ± 0.17
Taizhou	0.58 ± 0.07	0.55 ± 0.12	0.80 ± 0.12	0.70 ± 0.17	0.61 ± 0.09	0.62 ± 0.16	0.38 ± 0.03	0.37 ± 0.11	0.55 ± 0.06	0.52 ± 0.15
Suqian	0.52 ± 0.06	0.53 ± 0.10	0.79 ± 0.13	0.70 ± 0.18	0.47 ± 0.07	0.56 ± 0.15	0.29 ± 0.02	0.32 ± 0.10	0.51 ± 0.04	0.55 ± 0.17
Jiangsu Province	0.58 ± 0.06	0.56 ± 0.11	0.83 ± 0.12	0.75 ± 0.16	0.56 ± 0.08	0.60 ± 0.15	0.34 ± 0.02	0.33 ± 0.06	0.58 ± 0.05	0.54 ± 0.14

Seasonally, the 0.30–0.45 bin exhibited the highest NO_2 and SO_2 occurrence frequencies in summer and the lowest in winter (Figure 3). Particularly in summer, for the 0.30–0.45 bin, the occurrence frequency of NO_2 was highest in Zhenjiang (54.09%) and lowest in Suqian, whereas SO_2 was highest in Suzhou and Zhenjiang (25%) and reached its lowest in Yancheng. For the same bin in the winter, the occurrence frequency of NO_2 was comparatively highest in Yancheng (18.85%) and lowest in Wuxi, whereas SO_2 showed its highest in Yancheng (20.37%) and lowest in Nanjing. The significant anthropogenic emissions in China, including coal burning for room heating in winter, along with favorable meteorological conditions, are possibly responsible for the high level of pollutions [81,82]. Furthermore, the 0.45–0.60 bin showed the highest occurrence frequencies of NO_2 and SO_2 in spring and the lowest in summer (Figure 3). For the 0.45−0.60 bin in the spring, the occurrence frequency of NO_2 was highest in Suqian (20.32%) and lowest in Suzhou, whereas SO_2 was highest in Huaian (19.51%) and lowest in Zhenjiang. Similarly, in summer, the occurrence frequency of NO_2 was highest in Suzhou (26.21%) and lowest in Huaian, while SO_2 showed its highest frequency in Zhenjiang (12.50%) and lowest in Lianyungang. Notably, in winter, a high level of pollution was identified, as indicated by the >1.2 bin, accounting for the occurrence frequency of NO_2 of <32.46% and SO_2 of <21.67% for the 13 cities of Jiangsu Province.
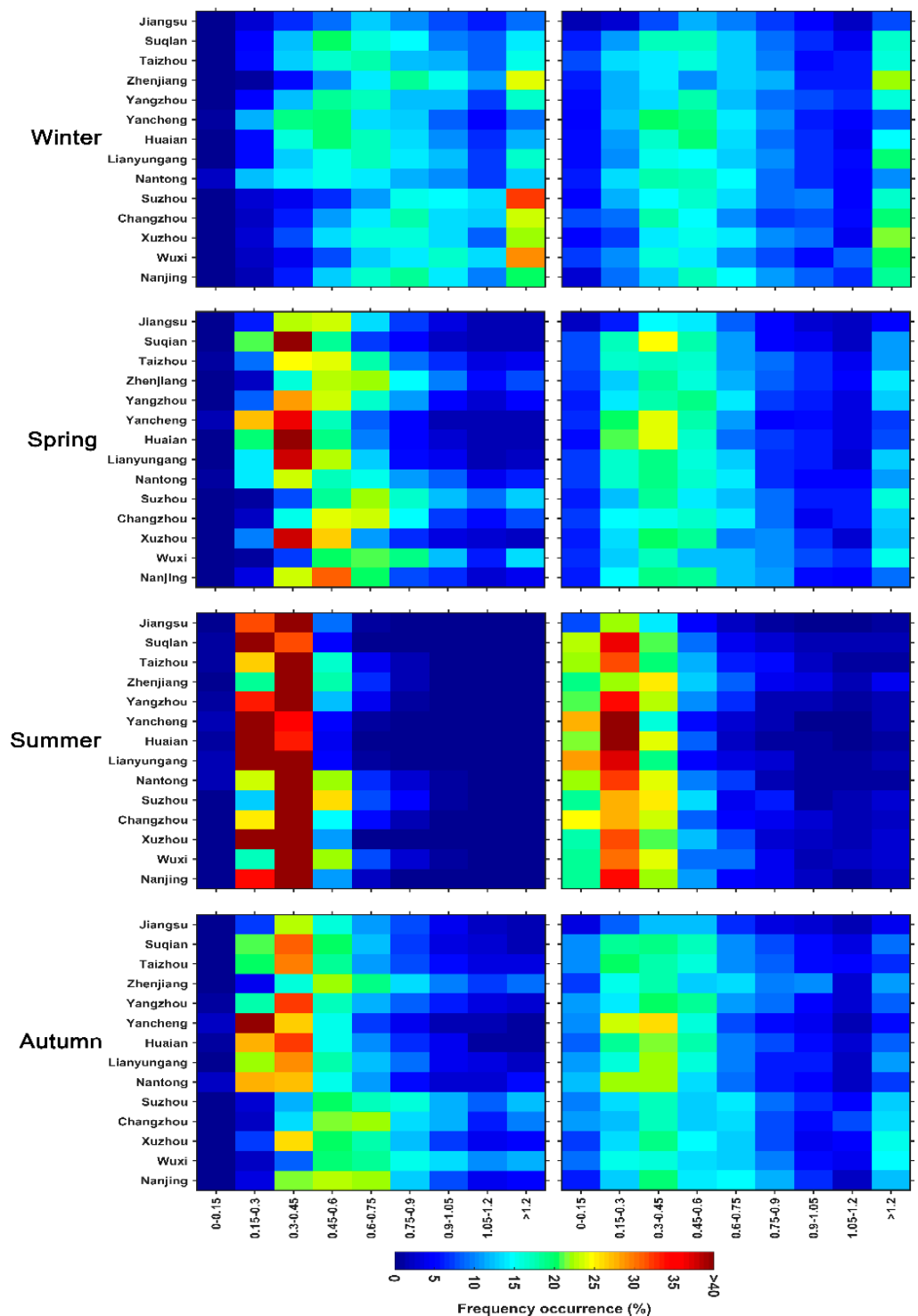

Figure 3. *Cont*.

Figure 3. Annual and seasonal frequency distributions of OMI-retrieved total column NO$_2$ (DU) and SO$_2$ (DU) in 13 cities of Jiangsu Province from 2005 to 2020.

3.3. Ratio of SO$_2$/NO$_2$ Indicator for Pollution Level

The SO$_2$/NO$_2$ ratio was used to examine the sources of air pollutants (mobile sources such as traffic emissions and point sources such as industrial activities) [83], as well as to evaluate the performance of the fuel gas desulfurization (FGD) device [20]. It was also used to detect the major contributors to air pollution in Jiangsu Province. A high SO$_2$/NO$_2$ ratio (>0.60) indicates significant contributions from point sources, while a low ratio (0.04~0.12) signifies more contributions from mobile sources [83,84]. High values of the SO$_2$/NO$_2$ ratio

(>0.60) suggest that the source of NO_2 and SO_2 pollutants were primarily from industry during the period of 2005−2020 (Figure 4). Significant annual and seasonal variations in SO_2/NO_2 ratios were observed in 13 cities of Jiangsu Province (Figure 5). In addition, the SO_2/NO_2 ratio peaked for a few specific years in the summer season, which may be due to less precipitation, resulting in the weakened rate of oxidation and wet deposition [23]. The SO_2/NO_2 ratio was located at >1 from 2005 to 2007 due to having uncontrolled NO_2 and SO_2 emissions from industry, and the ratio gradually decreased from 2008 after installation of the FGD device in the industry in 2007 (Figure 5). For the 13 studied cities, the 16-year city-level annual mean SO_2/NO_2 ratio was highest in Lianyungang and Yancheng (1.04) and lowest in Suzhou and Wuxi (0.78) (Figure 5 and Table S1). Moreover, the city-level significantly high correlations (r = 0.64~0.75) between NO_2 and SO_2 indicate that the source of NO_2 and SO_2 pollutants were from industrial activities (Table S2). Interestingly, the SO_2/NO_2 ratio values and correlation for the 13 cities of Jiangsu Province were remarkably close to one another, indicating the significant contributions from industrial activities to NO_2 and SO_2 emissions in Jiangsu Province (ratio = 0.97 and r = 0.78). These results suggest that industrial activities contribute to high SO_2 pollution over Lianyungang, Yancheng, Xuzhou, Huaian, and Suqian, perhaps due to the high-sulfur coals used [85]. The installation of the FGD device in the industry in 2007 reduced SO_2 emissions, resulting in manifestly lower concentrations in SO_2 relative to NO_2 over Jiangsu Province and the Yangzhou, Taizhou, Nanjing Nantong, Zhenjiang, Changzhou, Suzhou, and Wuxi cities. Li et al. [47] reported that the widespread installation of FGD devices in Chinese power plants was responsible for decreasing SO_2 emissions. Seasonally, the values of the SO_2/NO_2 ratio were highest in spring (0.83~1.22), followed by summer (0.88~1.15), autumn (0.74~1.10), and winter (0.68~0.95), in 13 cities of Jiangsu Province (Figures 4 and 5 and Table S1). In spring, the SO_2/NO_2 ratio was highest in Lianyungang (1.22) and reached its lowest in Suzhou and Wuxi (0.83). In summer, it was highest in Xuzhou (1.15) and lowest in Nantong (0.88) (Table S1). In autumn, the SO_2/NO_2 ratio reached its highest in Huaian (1.11) and lowest in Wuxi (0.74), while in winter, it was highest in Yancheng (0.95) and lowest in Suzhou (0.68).

3.4. NO_2 and SO_2 Trends

To get a clear understanding of changes in OMI-based total column NO_2 and SO_2 (DU), their spatial and city-level trends at annual and seasonal timescales were calculated for the 13 cities of Jiangsu Province. Trends in NO_2 and SO_2 concentrations were calculated for 2005–2020, 2006–2010 (when China introduced strict air pollution control policies during the 11th Five Year Plan (FYP)), 2011–2015 (during the 12th FYP), and 2013–2017 (Action Plan of Air Pollution Prevention and Control (APPC-AC)); see Figures 6–9 and Tables S3 and S4. The black dot (.) indicates tests of significance for NO_2 and SO_2 trends at a 95% confidence level. It is evident from Figures 6–9 and Tables S3 and S4 that not all cities have statistically significant trends. A noticeable spatial contrast in NO_2 and SO_2 trends (increasing and decreasing) was noticed during different periods (Figures 6 and 8). Notably, annually, decreasing trends in NO_2 (DU/year) were higher in magnitude for 2011–2015 (−0.024~−0.052) than in 2013-2017 (−0.007~−0.043), with the highest in Wuxi and the lowest in Yancheng (Figure 7). In contrast, increasing trends in NO_2 (0.015 to 0.031 per year) were seen during the 11th FYP period (2006–2010), with the highest in Nantong and the lowest in Suzhou. The stronger negative trends during 2011–2015 and 2013–2017 relative to the positive trends in 2006-2010 led to an overall decreasing trend in NO_2 (DU/year) during 2005 to 2020 (−0.002 to −0.012) throughout Jiangsu Province, except for Lianyungang (0.0003; Figure 7). The decreasing trend was highest in Suzhou and lowest in Suqian and Yancheng. As for the annual trends, NO_2 showed decreasing trends during 2005−2020, 2011−2015, and 2013−2017 and increasing trends in 2006–2010 for all seasons in 13 cities of Jiangsu Province (Table S3).
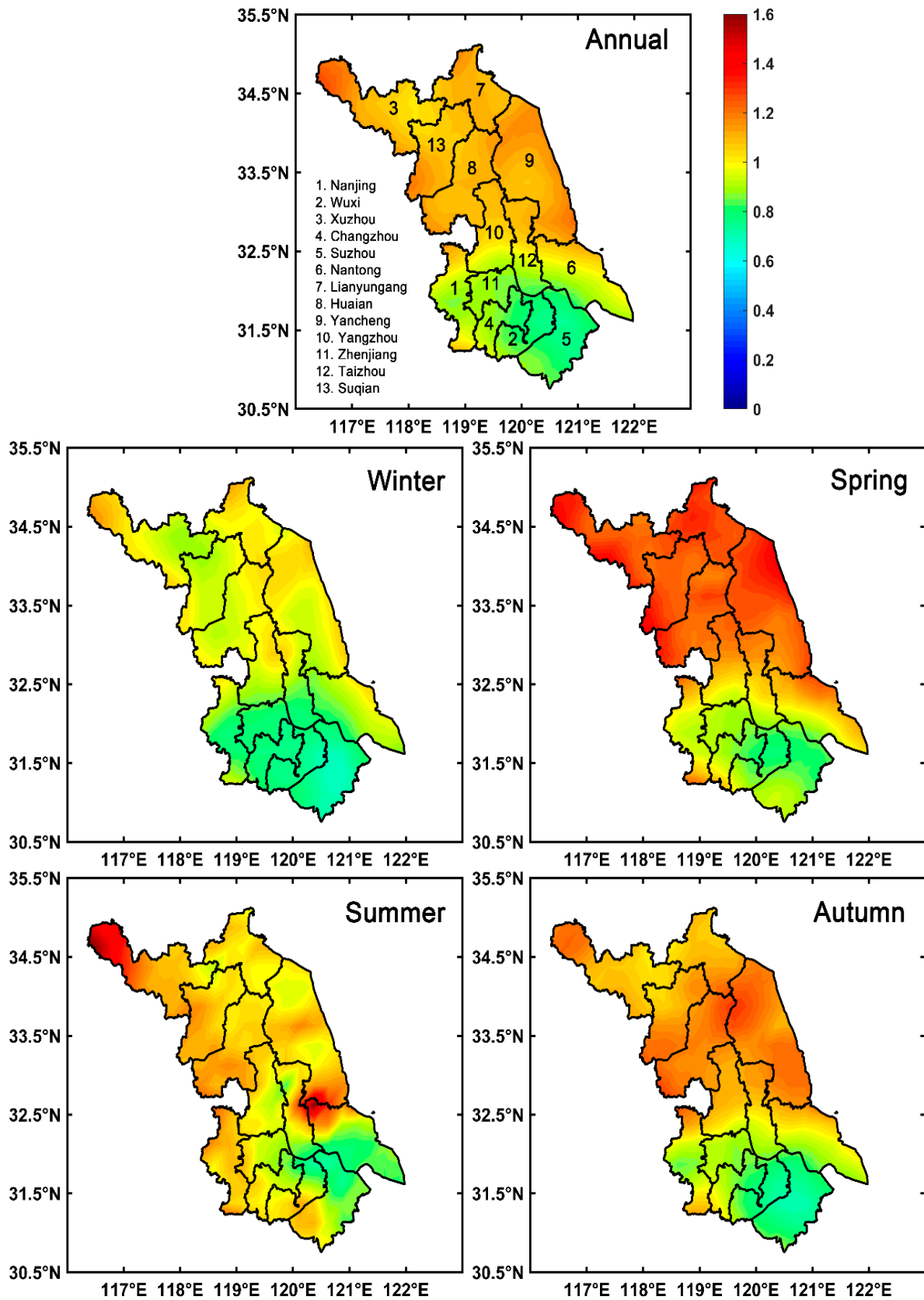
Figure 4. Annual and seasonal spatial distribution of the SO_2/NO_2 ratio, obtained from OMI, in 13 cities of Jiangsu Province from 2005 to 2020.
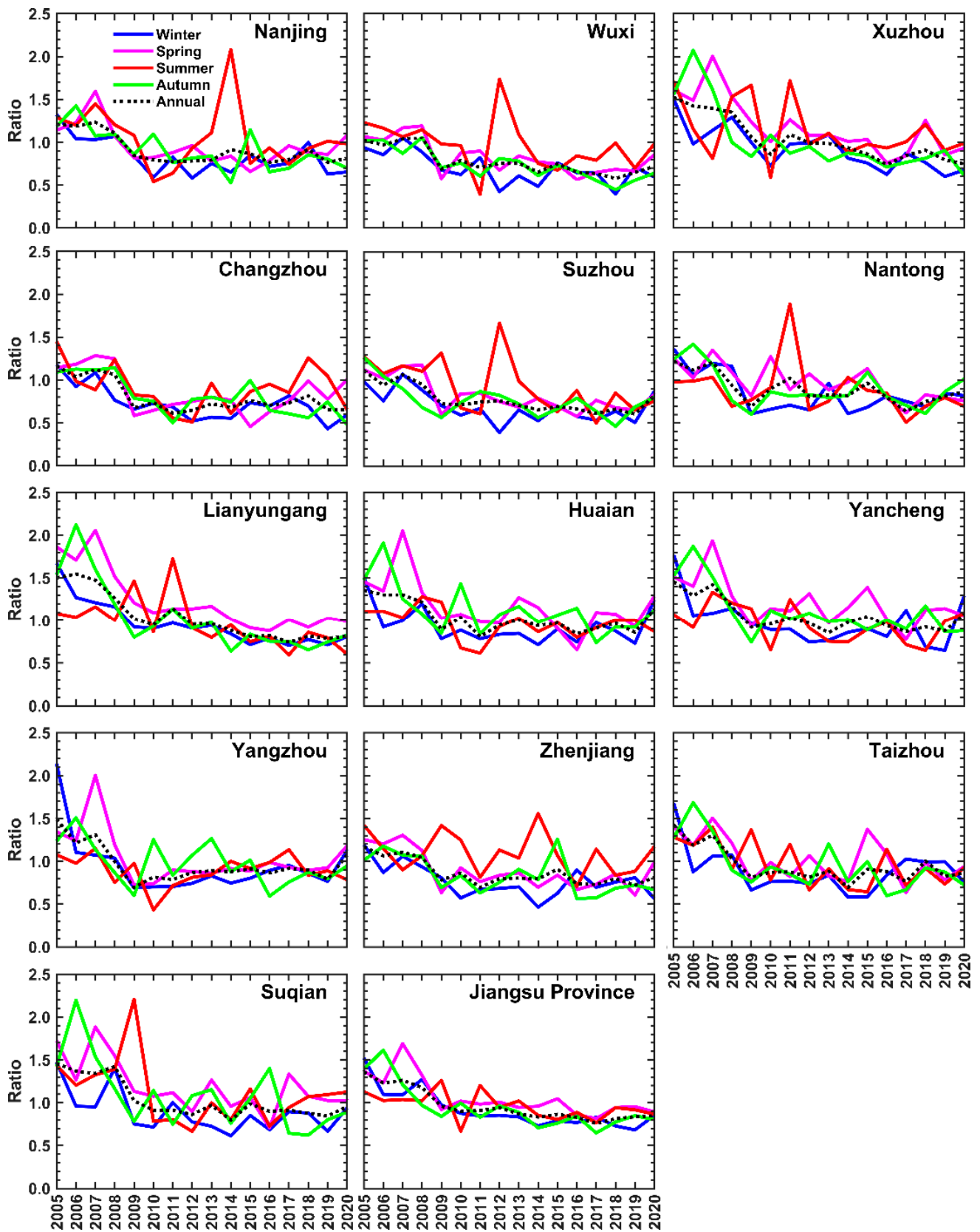
Figure 5. Annual and seasonal variations in the SO_2/NO_2 ratio, obtained from OMI, in 13 cities of Jiangsu Province from 2005 to 2020.
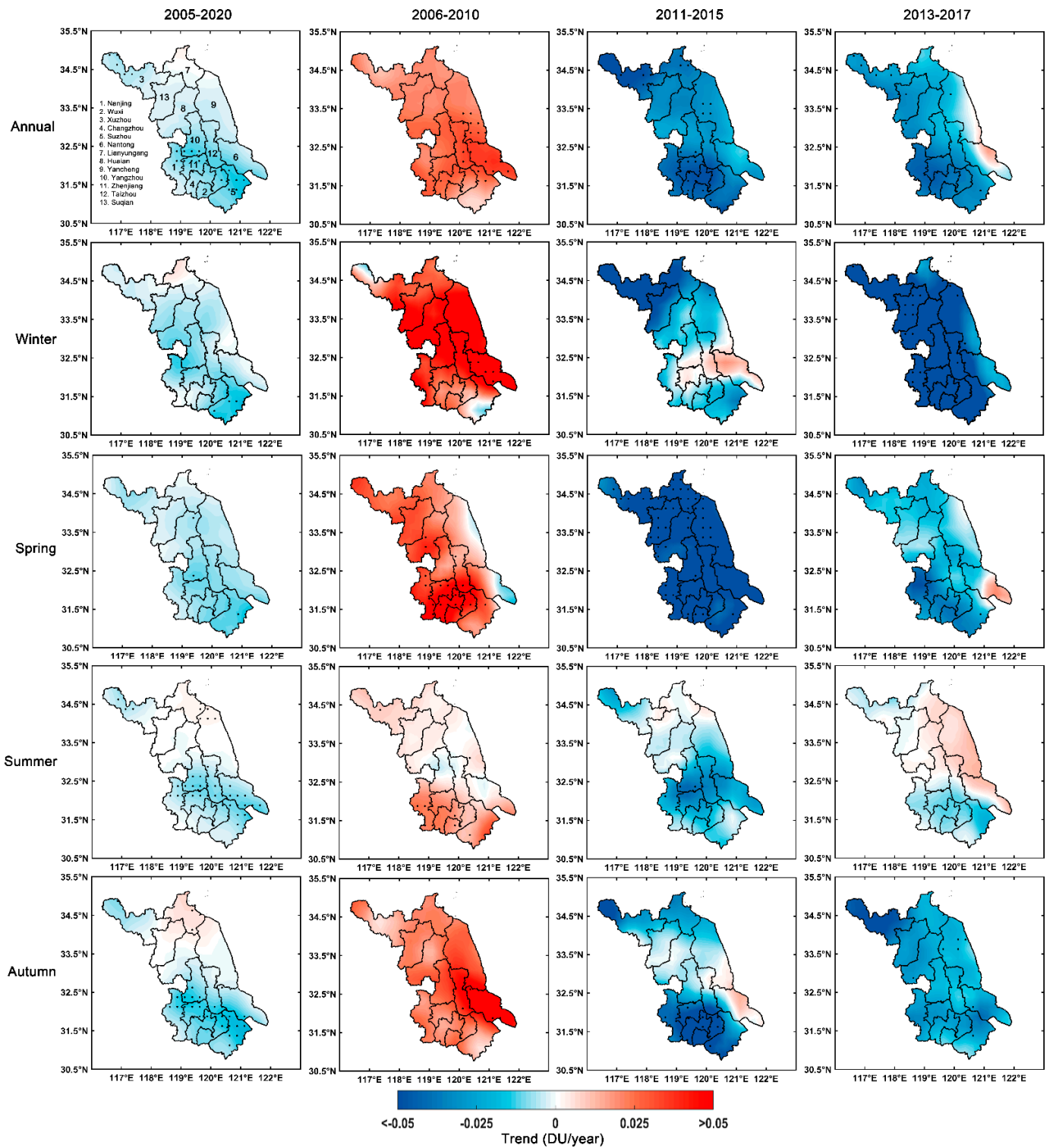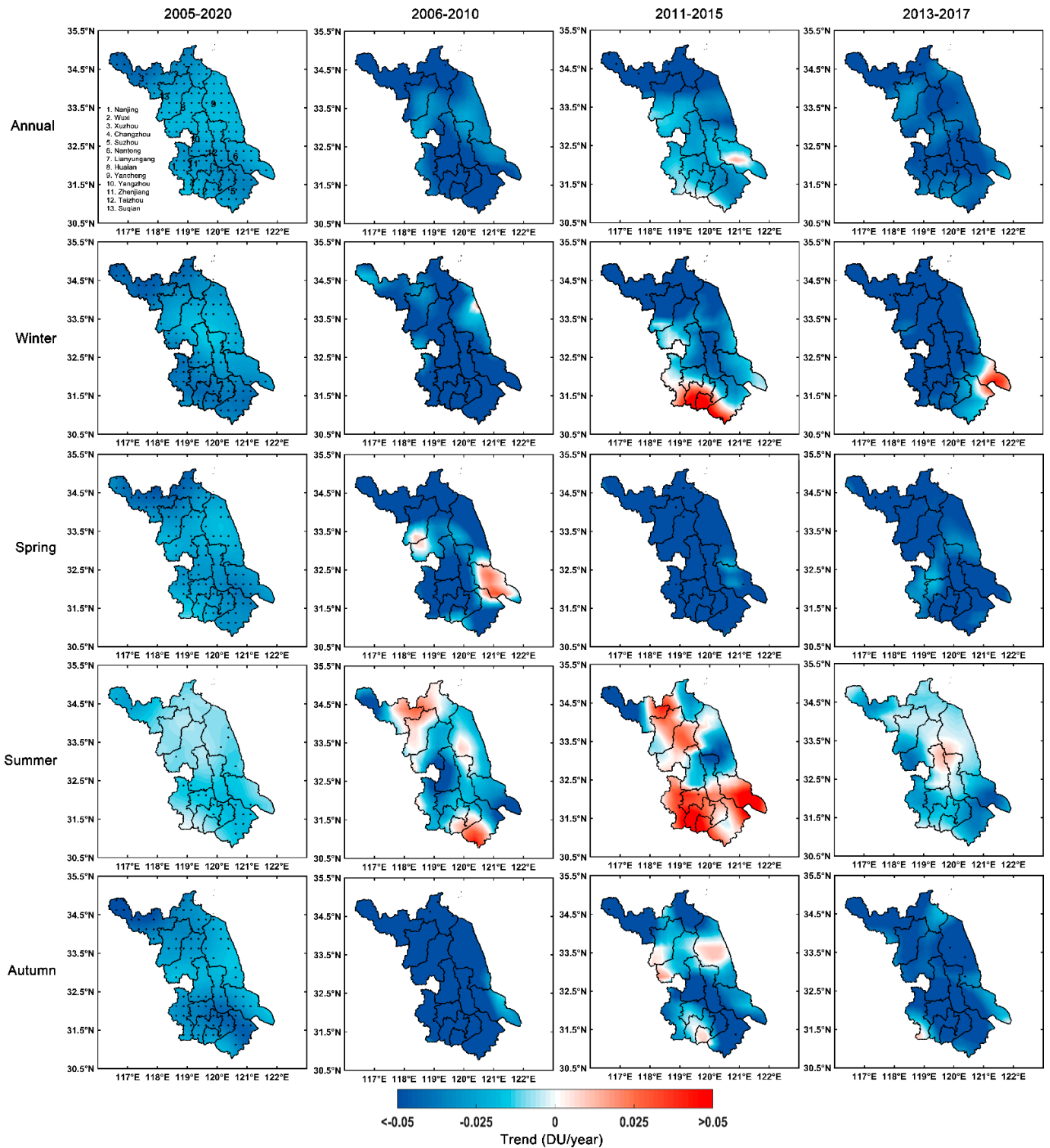
Figure 6. Annual and seasonal spatial trends in OMI-based total column NO$_2$ (DU/year) for the periods of 2005−2020, 2006−2010, 2011−2015, and 2013−2017 in Jiangsu Province. The dot (.) indicates significance at a 95% confidence level.
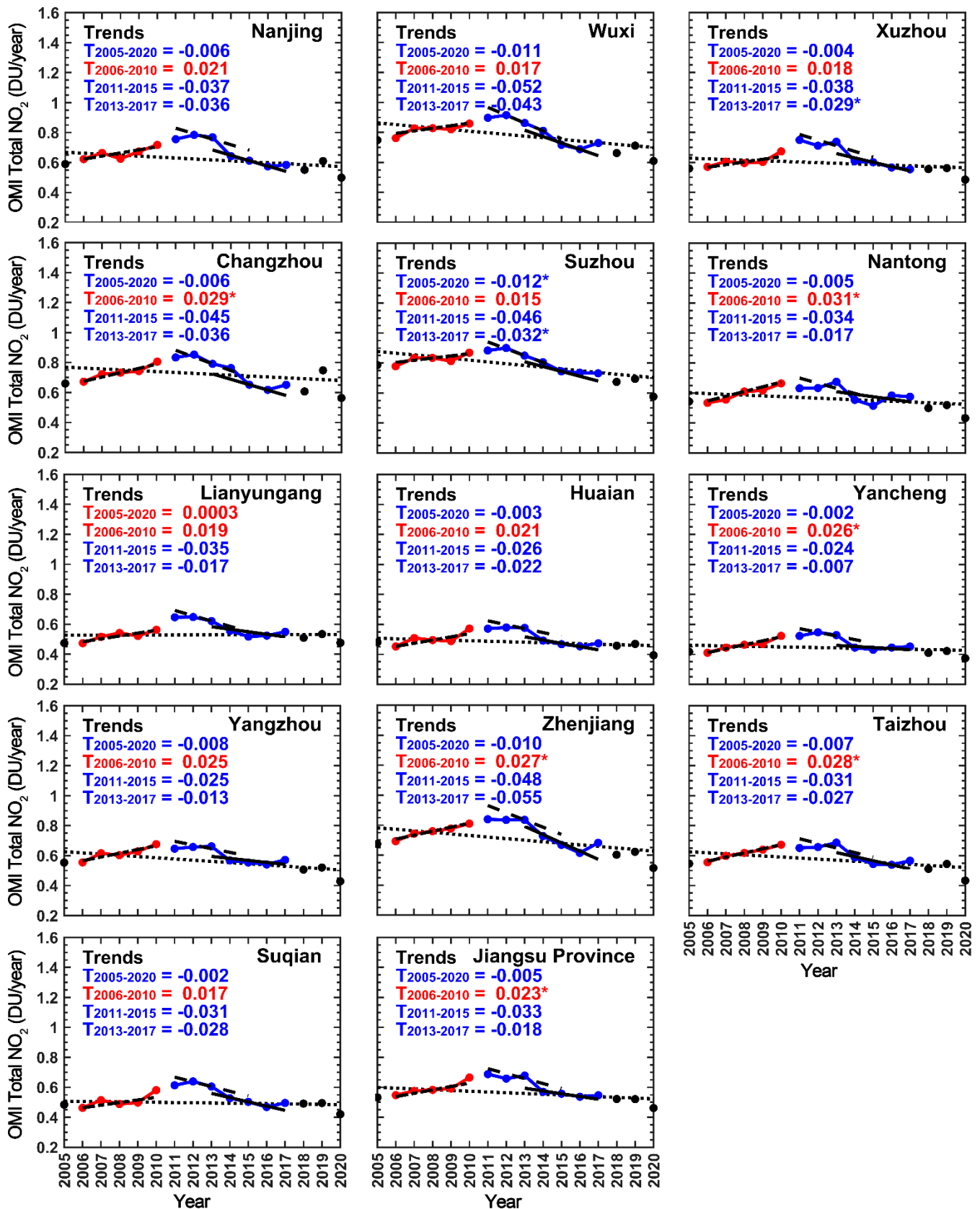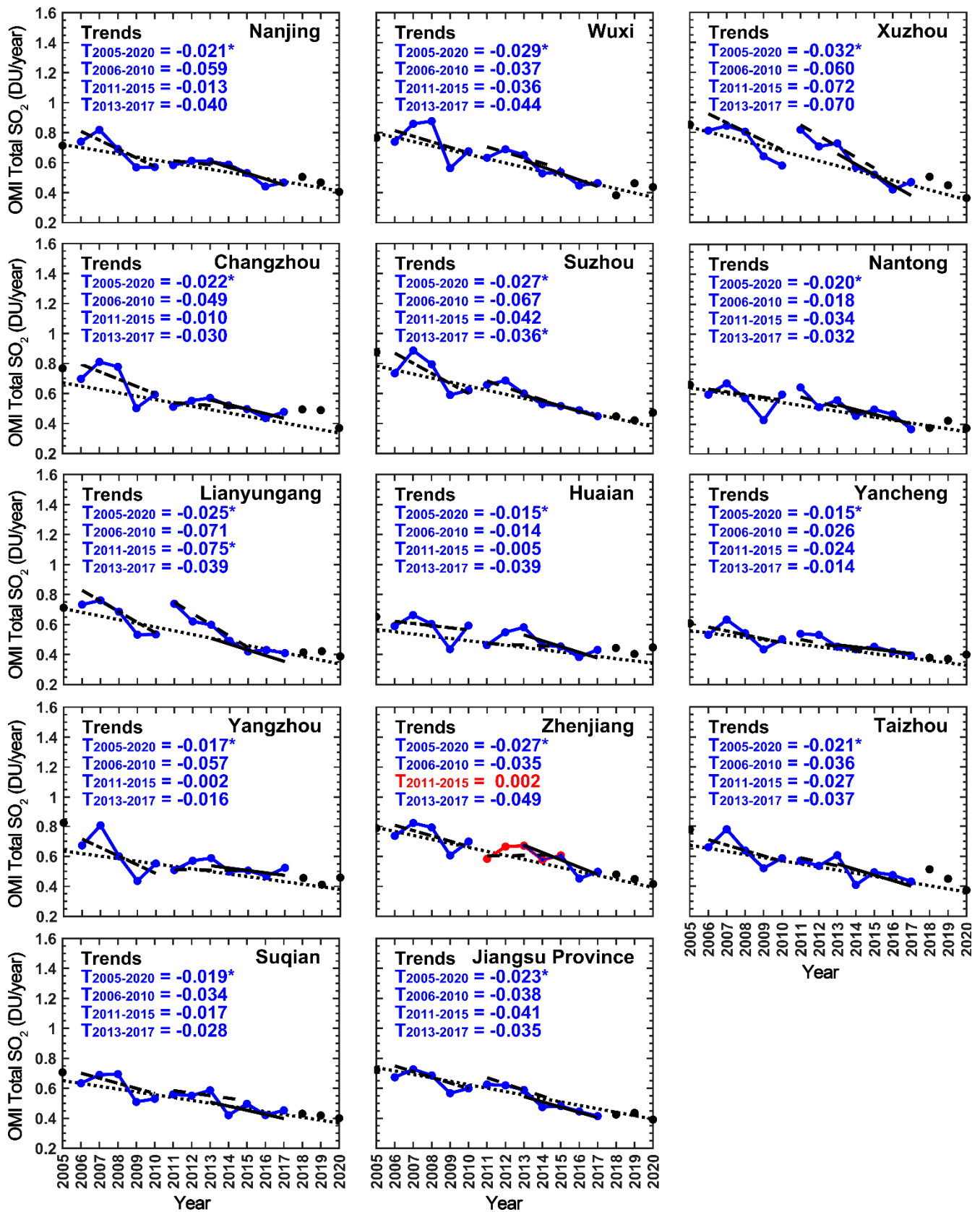
Figure 7. Trends in NO$_2$ (DU/year) for the periods of 2005−2020, 2006−2010, 2011−2015, and 2013−2017 in 13 cities of Jiangsu Province. The red color indicates an increasing trend, and the blue color indicates a decreasing trend in NO$_2$. The asterisk (*) indicates significance.

Figure 8. Annual and seasonal spatial trends in OMI-based total column SO$_2$ (DU/year) for the periods of 2005−2020, 2006−2010, 2011−2015, and 2013−2017 in Jiangsu Province. The dot (.) indicates significance at a 95% confidence level.

Figure 9. Trends in SO$_2$ (DU/year) for the periods of 2005−2020, 2006−2010, 2011−2015, and 2013−2017 in 13 cities of Jiangsu Province. The red color indicates an increasing trend, and the blue color indicates a decreasing trend in SO$_2$. The asterisk (*) indicates significance.

Furthermore, decreasing trends in SO_2 (DU/year) were higher during 2011–2015 (−0.002~−0.075) than in 2006–2010 (−0.014~−0.071), 2013–2017 (−0.007~−0.043), and 2005–2020 (−0.015~−0.032) for the 13 studied cities (Figure 9). In particular, during 2005–2020, the decreasing trend in SO_2 was highest in Xuzhou and lowest in Huaian and Yancheng, while during 2006–2010, the decreasing trend in SO_2 was highest in Lianyungang and lowest in Huaian. During 2011–2015, the decreasing trend in SO_2 peaked in Lianyungang and was weakest in Yangzhou. During 2013–2017, the decreasing trend in SO_2 was highest in Xuzhou and lowest in Yancheng. Seasonally, decreasing trends in SO_2 (DU/year) were more prominent during 2005–2020 for all seasons than in 2006–2010, 2011–2015, and 2013–2017 (Table S3). Several reasons are responsible for both increasing and decreasing trends in NO_2 and SO_2 during the study periods. For example, the implementation of desulfurization projects in coal-fired power plants started from the 11th FYP period (2006–2010) and continued for the 12th FYP (2011–2015) and APPC-AC (2013–2017) periods [47,86], resulting in decreasing trends in SO_2 during the study period. In contrast, there was no control policy implemented for reducing NO_2 emissions during the 11th FYP period (2006–2010) [86], resulting in increased NO_2 in that period, which is also visible in our study (see Figures 6 and 7). The implementation of denitration projects of coal-fired power plants started from the 12th FYP period (2011–2015), resulting in a substantial reduction in NO_2, which is evident in our study (see Figures 6 and 7). Apart from these, de Gouw et al. [87] reported a significant reduction in CO_2, NO_2, and SO_2 emissions due to installation of the combined cycle technology in Chinese coal-fired power plants and major industrial sectors. Zhao et al. [88] found a significantly larger reduction in NO_2 emissions in China during the 12th FYP period than during the 11th FYP period. According to the China Air Quality Management Assessment Report, a 6.7% reduction in NO_2 emission was estimated during 2013–2014 [89]. Gao et al. [90] reported that China's strict air pollution control policy cut 10% of national SO_2 emissions by 2010.

3.5. Source Identification of NO_2 and SO_2 Using PSCF Analysis

We used PSCF analysis, based on 72 h back trajectories obtained from the HYSPLIT model and surface measurements, to identify the potential source areas of NO_2 and SO_2 pollutants in Jiangsu Province. We conducted the HYSPLIT back-trajectory analysis for the period of 2014–2020, in which trajectories from all sites were used to compute a single PSCF for each air pollutant that presented the overall potential sources with all measurement sites treated as a whole. The results of the PSCF analysis are exhibited by seasons in Figure 10. In winter, high values of the PSCF (>0.5) were found in different parts of China, such as Anhui, Hebei, Henan, Hubei, Hunan, Jiangsu (cities of Nanjing, Changzhou, Suzhou, Wuxi, and Xuzhou), Jiangxi, Shandong, Shanxi, and Zhejiang, which are the potential source areas of NO_2 and SO_2 pollutants (Figure 10). PSCF values from 0.0 to 0.50 were found throughout China and in neighboring countries (e.g., Bangladesh, Kazakhstan, Mongolia, India, Nepal, Russia, and Tajikistan), and these were identified as moderate sources of NO_2 and SO_2. These results suggest that the local sources influence the wintertime air quality of Jiangsu Province much more significantly than do pollutants transported from outside. In spring, a high PSCF > 0.35 indicates that the potential source areas of NO_2 and SO_2 pollutants are located in Jiangsu and neighboring provinces (e.g., Anhui, Hubei, Hunan, Jiangxi, Shandong, and Zhejiang). In contrast, lower PSCF values (0.0~0.35) indicate other source areas of NO_2 and SO_2 pollutants located inside China and neighboring countries (e.g., Bangladesh, Kazakhstan, Mongolia, India, Nepal, Russia, and Tajikistan). This suggests that local sources also impact the springtime air quality of Jiangsu Province, along with outside sources, but contributions from local sources are lower than in winter. In summer, PSCF values (0.0~0.25) identify the potential sources of NO_2 and SO_2 pollutants across eastern China and outside of China (Mongolia, Russia), suggesting Jiangsu's air quality is affected by both local and remote sources, but pollution levels are lower than in winter and spring. In autumn, a high PSCF (>0.4) identified the potential source areas of NO_2 and SO_2 pollutants in most parts of China (e.g., Anhui, Hubei, Hunan, Jiangxi,

Shandong, and Zhejiang). PSCF (<0.40) values were lower throughout China and in neighboring countries (e.g., Bangladesh, Kazakhstan, Mongolia, India, Nepal, Russia, and Tajikistan) in autumn. This suggests that the autumn air quality of Jiangsu Province is significantly impacted by local sources more than by outside sources but that local sources are spatially weaker than in winter. Overall, we conclude that the air quality of Jiangsu Province is seriously impacted by local sources but also influenced by pollution transported from more distant regional source areas.
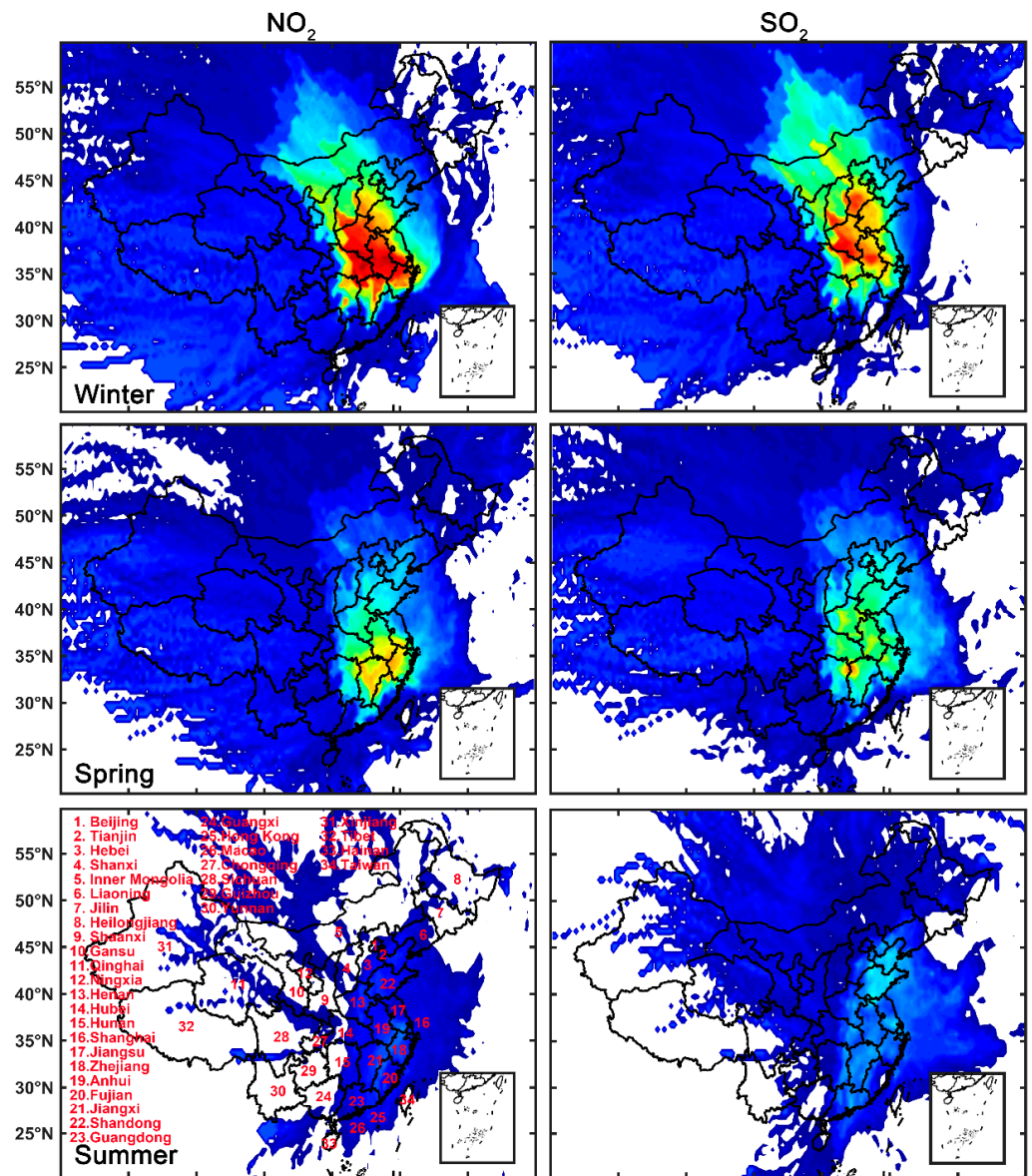
Figure 10. *Cont.*
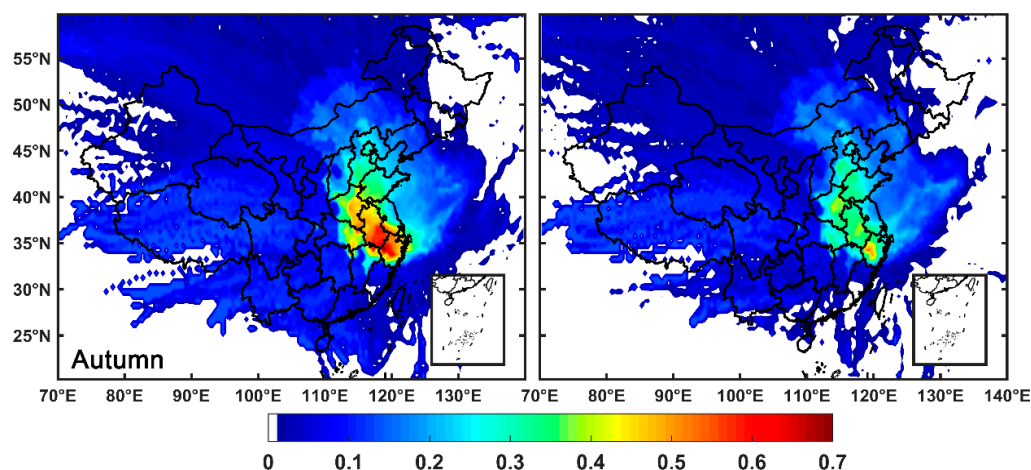
Figure 10. Source identification of NO_2 and SO_2 using the PSCF from 2014 to 2020 at annual and seasonal timescales in Jiangsu Province.

4. Conclusions

We examined long-term (2005–2020) spatiotemporal distributions and variations of NO_2 and SO_2 pollution and their ratio, trends, and sources (using PSCF analysis) in Jiangsu Province. Our major findings are as follows:

- The hotspots of NO_2 and SO_2 (DU) were found in most cities of Jiangsu Province, as indicated by high values of NO_2 and SO_2 (>0.60 DU). Long-term (2005–2020) city-level annual mean NO_2 showed its highest value in Wuxi and SO_2 in Xuzhou due to the dominance of local anthropogenic activities over these regions. However, both NO_2 and SO_2 found their lowest levels in Yancheng City.
- Seasonally, both NO_2 and SO_2 showed their highest values in winter due to increased anthropogenic emission activities (coal-based burning for room heating in the cold season) and stable atmospheric conditions (stagnant conditions and a shallower boundary layer). In contrast, both NO_2 and SO_2 were lowest in summer due to heavy precipitation, which washes out the pollution from the atmosphere.
- The occurrence frequencies of NO_2 and SO_2 were relatively common for the 0.3–0.6 bins. Notably, the high level of pollution across Jiangsu Province was identified by the NO_2 and SO_2 > 1.2 bin, and the occurrence frequency of NO_2 and SO_2 was highest in winter than in other seasons.
- High SO_2/NO_2 ratio values (>0.60) indicate industry as the dominant source, with significant annual and seasonal fluctuations. The long-term (2005–2020) SO_2/NO_2 ratio showed its highest in Lianyungang and Yancheng (1.04) and lowest in Suzhou and Wuxi (0.78), suggesting that industrial activities contribute to high SO_2 pollution due to the use of high-sulfur coals. Seasonally, the SO_2/NO_2 ratio was highest in spring (0.83~1.22), followed by summer (0.88~1.15), autumn (0.74~1.10), and winter (0.69~0.95).
- Annually, NO_2 showed decreasing trends (DU/year) at a larger magnitude during 2011-2015 (-0.024~-0.052) compared to 2013-2017 (-0.007~-0.043) and 2005–2020 (-0.002 to -0.012) and increasing trends during 2006–2010 (0.015 to 0.031). NO_2 also showed decreasing trends during 2005–2020, 2011–2015, and 2013–2017 and an increasing trend in 2006–2010 for all seasons.
- Decreasing trends in SO_2 (DU/year) were more prominent during 2011–2015 (-0.002~-0.075) than in 2006–2010 (-0.014~-0.071), 2013–2017 (-0.007~-0.043), and 2005–2020 (-0.015~-0.032). As with the annual trends, decreasing trends in SO_2 were also evident in all seasons.
- PSCF analysis indicated that Jiangsu's air quality is strongly affected by anthropogenic sources located inside China, with some contributions from neighboring countries (e.g., Bangladesh, Kazakhstan, Mongolia, India, Nepal, Russia, and Tajikistan).

Overall, this study facilitates understanding the level of SO_2 and NO_2 pollutions and can be considered as an environment supportive document for Jiangsu Province in China.

References

1. Wang, Y.; Ali, A.; Bilal, M.; Qiu, Z.; Ke, S.; Almazroui, M.; Islam, M.; Zhang, Y. Identification of Aerosol Pollution Hotspots in Jiangsu Province of China. *Remote Sens.* **2021**, *13*, 2842. [CrossRef]
2. Chan, C.K.; Yao, X. Air pollution in mega cities in China. *Atmos. Environ.* **2008**, *42*, 1–42. [CrossRef]
3. Li, F.; Song, Z.; Liu, W. China's energy consumption under the global economic crisis: Decomposition and sectoral analysis. *Energy Policy* **2014**, *64*, 193–202. [CrossRef]
4. Yuan, Y.; Liu, S.; Castro, R.; Pan, X. PM2.5 Monitoring and Mitigation in the Cities of China. *Environ. Sci. Technol.* **2012**, *46*, 3627–3628. [CrossRef]
5. Chang, Y. China Needs a Tighter PM2.5 Limit and a Change in Priorities. *Environ. Sci. Technol.* **2012**, *46*, 7069–7070. [CrossRef]
6. Hao, J.; Zhu, T.; Fan, X. Indoor Air Pollution and Its Control in China. In *Indoor Air Pollution. The Handbook of Environmental Chemistry*; Springer: Berlin/Heidelberg, Germany, 2014; Volume 64, pp. 145–170. [CrossRef]
7. Wang, S.W.; Zhang, Q.; Streets, D.G.; He, K.B.; Martin, R.V.; Lamsal, L.N.; Chen, D.; Lei, Y.; Lu, Z. Growth in NOx emissions from power plants in China: Bottom-up estimates and satellite observations. *Atmos. Chem. Phys. Discuss.* **2012**, *12*, 4429–4447. [CrossRef]
8. Slezakova, K.; Pires, J.; Martins, F.; Pereira, M.; Alvim-Ferraz, M. Identification of tobacco smoke components in indoor breathable particles by SEM–EDS. *Atmos. Environ.* **2011**, *45*, 863–872. [CrossRef]
9. WHO. Regional Office Air Quality Guidelines. In *Air Quality Guidelines for Europe*; WHO: Geneva, Switzerland, 2000.
10. IPCC. *Climate Change 2007. The Physical Science Basis: Working Group I Contribution to the Fourth Assessment Report of the IPCC., Science (80-.)*; Cambridge University Press: Cambridge, UK, 2007.
11. He, Y.; Uno, I.; Wang, Z.; Ohara, T.; Sugimoto, N.; Shimizu, A.; Richter, A.; Burrows, J.P. Variations of the increasing trend of tropospheric NO_2 over central east China during the past decade. *Atmos. Environ.* **2007**, *41*, 4865–4876. [CrossRef]
12. Shon, Z.-H.; Kim, K.-H.; Song, S.K. Long-term trend in NO_2 and NOx levels and their emission ratio in relation to road traffic activities in East Asia. *Atmos. Environ.* **2011**, *45*, 3120–3131. [CrossRef]

13. Kajino, M.; Ueda, H.; Sato, K.; Sakurai, T. Spatial distribution of the source-receptor relationship of sulfur in Northeast Asia. *Atmos. Chem. Phys. Discuss.* **2011**, *11*, 6475–6491. [CrossRef]

14. Richter, A.; Wittrock, F.; Burrows, J.P. SO2 measurements with SCIAMACHY. In *Proceedings of the European Space Agency*; ESA SP: Bremen, Germany, 2006.

15. Dickerson, R.R.; Li, C.; Li, Z.; Marufu, L.T.; Stehr, J.W.; McClure, B.; Krotkov, N.; Chen, H.; Wang, P.; Xia, X.; et al. Aircraft observations of dust and pollutants over northeast China: Insight into the meteorological mechanisms of transport. *J. Geophys. Res. Space Phys.* **2007**, *112*. [CrossRef]

16. Richter, A.; Burrows, J. Tropospheric NO$_2$ from GOME measurements. *Adv. Space Res.* **2002**, *29*, 1673–1683. [CrossRef]

17. Cheng, M.; Jiang, H.; Guo, Z. Evaluation of long-term tropospheric NO$_2$ columns and the effect of different ecosystem in Yangtze River Delta. *Procedia Environ. Sci.* **2012**, *13*, 1045–1056. [CrossRef]

18. Schumann, U.; Huntrieser, H. The global lightning-induced nitrogen oxides source. *Atmos. Chem. Phys. Discuss.* **2007**, *7*, 3823–3907. [CrossRef]

19. Vinken, G.C.M.; Boersma, K.F.; Maasakkers, J.D.; Adon, M.; Martin, R.V. Worldwide biogenic soil NOx emissions inferred from OMI NO$_2$ observations. *Atmos. Chem. Phys.* **2014**, *14*, 18. [CrossRef]

20. Zhang, L.; Lee, C.S.; Zhang, R.; Chen, L. Spatial and temporal evaluation of long term trend (2005–2014) of OMI retrieved NO$_2$ and SO$_2$ concentrations in Henan Province, China. *Atmos. Environ.* **2017**, *154*, 151–166. [CrossRef]

21. Krotkov, N.A.; McLinden, C.A.; Li, C.; Lamsal, L.N.; Celarier, E.A.; Marchenko, S.V.; Swartz, W.H.; Bucsela, E.J.; Joiner, J.; Duncan, B.N.; et al. Aura OMI observations of regional SO$_2$ and NO$_2$ pollution changes from 2005 to 2015. *Atmos. Chem. Phys. Discuss.* **2016**, *16*, 4605–4629. [CrossRef]

22. Haq, Z.U.; Tariq, S.; Ali, M. Tropospheric NO$_2$ Trends over South Asia during the Last Decade (2004–2014) Using OMI Data. *Adv. Meteorol.* **2015**, *2015*, 1–18. [CrossRef]

23. Zheng, C.; Zhao, C.; Li, Y.; Wu, X.; Zhang, K.; Gao, J.; Qiao, Q.; Ren, Y.; Zhang, X.; Chai, F. Spatial and temporal distribution of NO$_2$ and SO$_2$ in Inner Mongolia urban agglomeration obtained from satellite remote sensing and ground observations. *Atmos. Environ.* **2018**, *188*, 50–59. [CrossRef]

24. Guo, H.; Gu, X.; Ma, G.; Shi, S.; Wang, W.; Zuo, X.; Zhang, X. Spatial and temporal variations of air quality and six air pollutants in China during 2015–2017. *Sci. Rep.* **2019**, *9*, 1–11. [CrossRef]

25. Lin, J.-T.; McElroy, M.B. Detection from space of a reduction in anthropogenic emissions of nitrogen oxides during the Chinese economic downturn. *Atmos. Chem. Phys. Discuss.* **2011**, *11*, 8171–8188. [CrossRef]

26. Hilboll, A.; Richter, A.; Burrows, J.P. Long-term changes of tropospheric NO$_2$ over megacities derived from multiple satellite instruments. *Atmos. Chem. Phys. Discuss.* **2013**, *13*, 4145–4169. [CrossRef]

27. Zhang, L.; Jacob, D.J.; Boersma, K.F.; Jaffe, D.A.; Olson, J.R.; Bowman, K.W.; Worden, J.R.; Thompson, A.M.; Avery, M.A.; Cohen, R.C.; et al. Transpacific transport of ozone pollution and the effect of recent Asian emission increases on air quality in North America: An integrated analysis using satellite, aircraft, ozonesonde, and surface observations. *Atmos. Chem. Phys. Discuss.* **2008**, *8*, 6117–6136. [CrossRef]

28. Wang, S.; Xing, J.; Chatani, S.; Hao, J.; Klimont, Z.; Cofala, J.; Amann, M. Verification of anthropogenic emissions of China by satellite and ground observations. *Atmos. Environ.* **2011**, *45*, 6347–6358. [CrossRef]

29. Lu, Z.; Streets, D.; de Foy, B.; Krotkov, N. Ozone Monitoring Instrument Observations of Interannual Increases in SO$_2$ Emissions from Indian Coal-Fired Power Plants during 2005–2012. *Environ. Sci. Technol.* **2013**, *47*, 13993–14000. [CrossRef] [PubMed]

30. Burrows, J.P.; Weber, M.; Buchwitz, M.; Rozanov, V.; Ladstätter-Weißenmayer, A.; Richter, A.; DeBeek, R.; Hoogen, R.; Bramstedt, K.; Eichmann, K.-U.; et al. The Global Ozone Monitoring Experiment (GOME): Mission Concept and First Scientific Results. *J. Atmos. Sci.* **1999**, *56*, 151–175. [CrossRef]

31. Eisinger, M.; Burrows, J.P. Tropospheric sulfur dioxide observed by the ERS-2 GOME instrument. *Geophys. Res. Lett.* **1998**, *25*, 4177–4180. [CrossRef]

32. Bovensmann, H.; Burrows, J.P.; Buchwitz, M.; Frerick, J.; Noël, S.; Rozanov, V.V.; Chance, K.; Goede, A.P.H. SCIAMACHY: Mission Objectives and Measurement Modes. *J. Atmos. Sci.* **1999**, *56*, 127–150. [CrossRef]

33. Munro, R.; Anderson, C.; Callies, J.; Corpaccioli', E.; Eisinger, M.; Lang, R.; Lefebvre, A.; Livschitz, Y.; Albiñana, A.P. GOME-2 on MetOp. In *Proceedings of the European Space Agency*; ESA SP: Bremen, Germany, 2006.

34. Munro, R.; Lang, R.; Klaes, D.; Poli, G.; Retscher, C.; Lindstrot, R.; Huckle, R.; Lacan, A.; Grzegorski, M.; Holdak, A.; et al. The GOME-2 instrument on the Metop series of satellites: Instrument design, calibration, and level 1 data processing—an overview. *Atmos. Meas. Tech.* **2016**, *9*, 1279–1301. [CrossRef]

35. Levelt, P.; Hilsenrath, E.; Leppelmeier, G.; Oord, G.V.D.; Bhartia, P.; Tamminen, J.; De Haan, J.; Veefkind, J. Science objectives of the ozone monitoring instrument. *IEEE Trans. Geosci. Remote. Sens.* **2006**, *44*, 1199–1208. [CrossRef]

36. Levelt, P.; Oord, G.V.D.; Dobber, M.; Malkki, A.; Visser, H.; De Vries, J.; Stammes, P.; Lundell, J.; Saari, H. The ozone monitoring instrument. *IEEE Trans. Geosci. Remote. Sens.* **2006**, *44*, 1093–1101. [CrossRef]

37. Veefkind, J.; Aben, I.; McMullan, K.; Förster, H.; de Vries, J.; Otter, G.; Claas, J.; Eskes, H.; de Haan, J.; Kleipool, Q.; et al. TROPOMI on the ESA Sentinel-5 Precursor: A GMES mission for global observations of the atmospheric composition for climate, air quality and ozone layer applications. *Remote Sens. Environ.* **2012**, *120*, 70–83. [CrossRef]

38. Levelt, P.F.; Joiner, J.; Tamminen, J.; Veefkind, J.P.; Bhartia, P.K.; Zweers, D.C.S.; Duncan, B.N.; Streets, D.G.; Eskes, H.; van der A, R.; et al. The Ozone Monitoring Instrument: Overview of 14 years in space. *Atmos. Chem. Phys. Discuss.* **2018**, *18*, 5699–5745. [CrossRef]

39. Damiani, A.; De Simone, S.; Rafanelli, C.; Cordero, R.; Laurenza, M. Three years of ground-based total ozone measurements in the Arctic: Comparison with OMI, GOME and SCIAMACHY satellite data. *Remote Sens. Environ.* **2012**, *127*, 162–180. [CrossRef]

40. Celarier, E.A.; Brinksma, E.J.; Gleason, J.F.; Veefkind, J.P.; Cede, A.; Herman, J.; Ionov, D.; Goutail, F.; Pommereau, J.-P.; Lambert, J.-C.; et al. Validation of Ozone Monitoring Instrument nitrogen dioxide columns. *J. Geophys. Res. Space Phys.* **2008**, *113*. [CrossRef]

41. Penn, E.; Holloway, T. Evaluating current satellite capability to observe diurnal change in nitrogen oxides in preparation for geostationary satellite missions. *Environ. Res. Lett.* **2020**, *15*, 034038. [CrossRef]

42. Lamsal, L.N.; Duncan, B.N.; Yoshida, Y.; Krotkov, N.; Pickering, K.E.; Streets, D.G.; Lu, Z.U.S. NO_2 trends (2005–2013): EPA Air Quality System (AQS) data versus improved observations from the Ozone Monitoring Instrument (OMI). *Atmos. Environ.* **2015**, *110*, 130–143. [CrossRef]

43. Van Der A, R.J.; Mijling, B.; Ding, J.; Koukouli, M.E.; Liu, F.; Li, Q.; Mao, H.; Theys, N. Cleaning up the air: Effectiveness of air quality policy for SO_2 and NOx emissions in China. *Atmos. Chem. Phys. Discuss.* **2017**, *17*, 1775–1789. [CrossRef]

44. Liu, F.; Zhang, Q.; Van Der A, R.J.; Zheng, B.; Tong, D.; Yan, L.; Zheng, Y.; He, K. Recent reduction in NO x emissions over China: Synthesis of satellite observations and emission inventories. *Environ. Res. Lett.* **2016**, *11*, 114002. [CrossRef]

45. Liu, F.; Beirle, S.; Zhang, Q.; Van Der A, R.J.; Zheng, B.; Tong, D.; He, K. NOx emission trends over Chinese cities estimated from OMI observations during 2005 to 2015. *Atmos. Chem. Phys. Discuss.* **2017**, *17*, 9261–9275. [CrossRef] [PubMed]

46. Cui, Y.; Lin, J.; Song, C.; Liu, M.; Yan, Y.; Xu, Y.; Huang, B. Rapid growth in nitrogen dioxide pollution over Western China, 2005–2013. *Atmos. Chem. Phys. Discuss.* **2016**, *16*, 6207–6221. [CrossRef]

47. Li, C.; Zhang, Q.; Krotkov, N.A.; Streets, D.G.; He, K.; Tsay, S.-C.; Gleason, J.F. Recent large reduction in sulfur dioxide emissions from Chinese power plants observed by the Ozone Monitoring Instrument. *Geophys. Res. Lett.* **2010**, *37*. [CrossRef]

48. Li, C.; McLinden, C.; Fioletov, V.; Krotkov, N.; Carn, S.; Joiner, J.; Streets, D.; He, H.; Ren, X.; Li, Z.; et al. India Is Overtaking China as the World's Largest Emitter of Anthropogenic Sulfur Dioxide. *Sci. Rep.* **2017**, *7*, 1–7. [CrossRef] [PubMed]

49. Wang, C.; Wang, T.; Wang, P.; Rakitin, V. Comparison and Validation of TROPOMI and OMI NO_2 Observations over China. *Atmosphere* **2020**, *11*, 636. [CrossRef]

50. Wang, Y.; Beirle, S.; Lampel, J.; Koukouli, M.; De Smedt, I.; Theys, N.; Li, A.; Wu, D.; Xie, P.; Liu, C.; et al. Validation of OMI, GOME-2A and GOME-2B tropospheric NO_2, SO_2 and HCHO products using MAX-DOAS observations from 2011 to 2014 in Wuxi, China: Investigation of the effects of priori profiles and aerosols on the satellite products. *Atmos. Chem. Phys. Discuss.* **2017**, *17*, 5007–5033. [CrossRef]

51. Song, R.; Yang, L.; Liu, M.; Li, C.; Yang, Y. Spatiotemporal Distribution of Air Pollution Characteristics in Jiangsu Province, China. *Adv. Meteorol.* **2019**, *2019*, 1–14. [CrossRef]

52. Qiu, Z.; Ali, A.; Nichol, J.; Bilal, M.; Tiwari, P.; Habtemicheal, B.; Almazroui, M.; Mondal, S.; Mazhar, U.; Wang, Y.; et al. Spatiotemporal Investigations of Multi-Sensor Air Pollution Data over Bangladesh during COVID-19 Lockdown. *Remote Sens.* **2021**, *13*, 877. [CrossRef]

53. He, L.; Zhong, Z.; Yin, F.; Wang, D. Impact of Energy Consumption on Air Quality in Jiangsu Province of China. *Sustainability* **2018**, *10*, 94. [CrossRef]

54. Torres, O.; Ahn, C.; Chen, Z. Improvements to the OMI near-UV aerosol algorithm using A-train CALIOP and AIRS observations. *Atmos. Meas. Tech.* **2013**, *6*, 3257–3270. [CrossRef]

55. Torres, O.; Tanskanen, A.; Veihelmann, B.; Ahn, C.; Braak, R.; Bhartia, P.K.; Veefkind, P.; Levelt, P. Aerosols and surface UV products form Ozone Monitoring Instrument observations: An overview. *J. Geophys. Res. Atmos.* **2007**, *112*. [CrossRef]

56. Ahmad, S.P.; Levelt, P.F.; Hilsenrath, E.; Tamminen, J.; Bhartia, P.; Veefkind, P.J.; Van Den Oord, B.; Joiner, J.; Fleig, A.; Johnson, J.; et al. Atmospheric Trace Gases, Aerosols, and Cloud Data from the EOS Ozone Monitoring Instrument (OMI) on the Aura Satellite. *AGU Fall Meet. Abstr.* **2005**, *2005*, A41A-0023.

57. Carn, S.A.; Fioletov, V.E.; McLinden, C.; Li, C.; Krotkov, N. A decade of global volcanic SO_2 emissions measured from space. *Sci. Rep.* **2017**, *7*, srep44095. [CrossRef]

58. Krotkov, N.A.; Lamsal, L.N.; Celarier, E.A.; Swartz, W.H.; Marchenko, S.V.; Bucsela, E.J.; Chan, K.L.; Wenig, M. The version 3 OMI NO_2 standard product. *Atmos. Meas. Tech. Discuss.* **2017**, *10*, 9. [CrossRef]

59. Li, C.; Krotkov, N.A.; Carn, S.; Zhang, Y.; Spurr, R.J.D.; Joiner, J. New-generation NASA Aura Ozone Monitoring Instrument (OMI) volcanic SO_2 dataset: Algorithm description, initial results, and continuation with the Suomi-NPP Ozone Mapping and Profiler Suite (OMPS). *Atmos. Meas. Tech.* **2017**, *10*, 445–458. [CrossRef]

60. Li, L.; Wu, J.; Ghosh, J.K.; Ritz, B. Estimating spatiotemporal variability of ambient air pollutant concentrations with a hierarchical model. *Atmos. Environ.* **2013**, *71*, 54–63. [CrossRef]

61. Veefkind, J.; De Haan, J.; Brinksma, E.; Kroon, M.; Levelt, P. Total ozone from the ozone monitoring instrument (OMI) using the DOAS technique. *IEEE Trans. Geosci. Remote Sens.* **2006**, *44*, 1239–1244. [CrossRef]

62. Bilal, M.; Mhawish, A.; Nichol, J.E.; Qiu, Z.; Nazeer, M.; Ali, A.; de Leeuw, G.; Levy, R.C.; Wang, Y.; Chen, Y.; et al. Air pollution scenario over Pakistan: Characterization and ranking of extremely polluted cities using long-term concentrations of aerosols and trace gases. *Remote. Sens. Environ.* **2021**, *264*, 112617. [CrossRef]

63. Mann, H.B. Nonparametric Tests Against Trend. *Econometrica* **1945**, *13*, 245. [CrossRef]
64. Kendall, M.G. *Rank Correlation Methods*, 4th ed.; Charles Griffin: Granville, OH, USA, 1975; ISBN 0195208374.
65. Sen, P.K. Journal of the American Statistical Estimates of the Regression Coefficient Based on Kendall's Tau. *J. Am. Stat. Assoc.* **1968**, *63*, 324. [CrossRef]
66. Stein, A.F.; Draxler, R.R.; Rolph, G.D.; Stunder, B.J.B.; Cohen, M.; Ngan, F. NOAA's HYSPLIT Atmospheric Transport and Dispersion Modeling System. *Bull. Am. Meteorol. Soc.* **2015**, *96*, 2059–2077. [CrossRef]
67. Fleming, Z.L.; Monks, P.; Manning, A.J. Review: Untangling the influence of air-mass history in interpreting observed atmospheric composition. *Atmos. Res.* **2011**, *104–105*, 1–39. [CrossRef]
68. Begum, B.A.; Kim, E.; Jeong, C.-H.; Lee, D.-W.; Hopke, P.K. Evaluation of the potential source contribution function using the 2002 Quebec forest fire episode. *Atmos. Environ.* **2005**, *39*, 3719–3724. [CrossRef]
69. Wang, Y.Q.; Zhang, X.Y.; Draxler, R.R. TrajStat: GIS-based software that uses various trajectory statistical analysis methods to identify potential sources from long-term air pollution measurement data. *Environ. Model. Softw.* **2009**, *24*, 938–939. [CrossRef]
70. Shah, V.; Jacob, D.; Li, K.; Silvern, R.; Zhai, S.; Liu, M.; Lin, J.; Zhang, Q. Effect of changing NOx lifetime on the seasonality and long-term trends of satellite-observed tropospheric NO_2 columns over China. *Atmos. Chem. Phys. Discuss.* **2019**, *20*, 1483–1495. [CrossRef]
71. Lee, C.; Martin, R.; Van Donkelaar, A.; Lee, H.; Dickerson, R.; Hains, J.C.; Krotkov, N.; Richter, A.; Vinnikov, K.; Schwab, J.J. SO_2 emissions and lifetimes: Estimates from inverse modeling using in situ and global, space-based (SCIAMACHY and OMI) observations. *J. Geophys. Res. Space Phys.* **2011**, *116*. [CrossRef]
72. Dahiya, S.; Myllyvirta, S. Global SO_2 emission hotspot database, Ranking the world's worst sources of SO_2 pollution. *Greenpeace Environ. Trust* **2019**, 1–13.
73. Lamsal, L.N.; Martin, R.; Parrish, D.D.; Krotkov, N. Scaling Relationship for NO_2 Pollution and Urban Population Size: A Satellite Perspective. *Environ. Sci. Technol.* **2013**, *47*, 7855–7861. [CrossRef] [PubMed]
74. Streets, D.G.; Yarber, K.F.; Woo, J.-H.; Carmichael, G.R. Biomass burning in Asia: Annual and seasonal estimates and atmospheric emissions. *Glob. Biogeochem. Cycles* **2003**, *17*. [CrossRef]
75. Wang, Y.; McElroy, M.B.; Palmer, P.I. Asian emissions of CO and NOx: Constraints from aircraft and Chinese station data. *J. Geophys. Res. Space Phys.* **2004**, *109*. [CrossRef]
76. Li, M.; Zhang, Q.; Kurokawa, J.-I.; Woo, J.-H.; He, K.; Lu, Z.; Ohara, T.; Song, Y.; Streets, D.G.; Carmichael, G.R.; et al. MIX: A mosaic Asian anthropogenic emission inventory under the international collaboration framework of the MICS-Asia and HTAP. *Atmos. Chem. Phys. Discuss.* **2017**, *17*, 935–963. [CrossRef]
77. Zheng, F.; Yu, T.; Cheng, T.; Gu, X.; Guo, H. Intercomparison of tropospheric nitrogen dioxide retrieved from Ozone Monitoring Instrument over China. *Atmos. Pollut. Res.* **2014**, *5*, 686–695. [CrossRef]
78. Meng, Z.-Y.; Xu, X.-B.; Wang, T.; Zhang, X.-Y.; Yu, X.-L.; Wang, S.-F.; Lin, W.-L.; Chen, Y.-Z.; Jiang, Y.-A.; An, X.-Q. Ambient sulfur dioxide, nitrogen dioxide, and ammonia at ten background and rural sites in China during 2007–2008. *Atmos. Environ.* **2010**, *44*, 2625–2631. [CrossRef]
79. Xue, R.; Wang, S.; Li, D.; Zou, Z.; Chan, K.L.; Valks, P.; Saiz-Lopez, A.; Zhou, B. Spatio-temporal variations in NO_2 and SO_2 over Shanghai and Chongming Eco-Island measured by Ozone Monitoring Instrument (OMI) during 2008–2017. *J. Clean. Prod.* **2020**, *258*, 120563. [CrossRef]
80. Feng, Z.; Huang, Y.; Feng, Y.; Ogura, N.; Zhang, F. Chemical Composition of Precipitation in Beijing Area, Northern China. *Water Air Soil Pollut.* **2001**, *125*, 345–356. [CrossRef]
81. Wang, Z.; Zheng, F.; Zhang, W.; Wang, S. Analysis of SO_2 Pollution Changes of Beijing-Tianjin-Hebei Region over China Based on OMI Observations from 2006 to 2017. *Adv. Meteorol.* **2018**, *2018*, 1–15. [CrossRef]
82. Wang, C.; Wang, T.; Wang, P. The Spatial–Temporal Variation of Tropospheric NO_2 over China during 2005 to 2018. *Atmosphere* **2019**, *10*, 444. [CrossRef]
83. Aneja, V.P.; Agarwal, A.; A Roelle, P.; Phillips, S.B.; Tong, Q.; Watkins, N.; Yablonsky, R. Measurements and analysis of criteria pollutants in New Delhi, India. *Environ. Int.* **2001**, *27*, 35–42. [CrossRef]
84. Halim, N.D.A.; Latif, M.T.; Ahamad, F.; Dominick, D.; Chung, J.X.; Juneng, L.; Khan, F. The long-term assessment of air quality on an island in Malaysia. *Heliyon* **2018**, *4*, e01054. [CrossRef]
85. Wang, T.; Cheung, T.F.; Li, Y.S.; Yu, X.M.; Blake, D.R. Emission characteristics of CO, NOx, SO_2 and indications of biomass burning observed at a rural site in eastern China. *J. Geophys. Res. Space Phys.* **2002**, *107*, 4157. [CrossRef]
86. Ma, Z.; Liu, R.; Liu, Y.; Bi, J. Effects of air pollution control policies on PM2.5 pollution improvement in China from 2005 to 2017: A satellite-based perspective. *Atmos. Chem. Phys. Discuss.* **2019**, *19*, 6861–6877. [CrossRef]
87. de Gouw, J.A.; Parrish, D.D.; Frost, G.J.; Trainer, M. Reduced emissions of CO 2, NOx, and SO 2 from U.S. power plants owing to switch from coal to natural gas with combined cycle technology. *Earth's Futur.* **2014**, *2*, 75–82. [CrossRef]
88. Zhao, B.; Wang, S.; Wang, J.; Fu, J.S.; Liu, T.; Xu, J.; Fu, X.; Hao, J. Impact of national NOx and SO_2 control policies on particulate matter pollution in China. *Atmos. Environ.* **2013**, *77*, 453–463. [CrossRef]
89. CAAC. *China Air Quality Management Assessment Report (2015)*; Secretariat for Clean Air Alliance of China: Beijing, China, 2015.
90. Gao, C.; Yin, H.; Ai, N.; Huang, Z. Historical Analysis of SO_2 Pollution Control Policies in China. *Environ. Manag.* **2009**, *43*, 447–457. [CrossRef] [PubMed]